RECLAMATION

Managing Water in the West

Desalination and Water Purification Research and Development Program Report No. 175

Novel Cylindrical Cross-Flow Hollow Fiber Membrane Module for Direct Contact Membrane Distillation-based Desalination

U.S. Department of the Interior
Bureau of Reclamation
Technical Service Center
Water and Environmental Services Division
Water Treatment Engineering Research Team
Denver, Colorado

October 2013

REPORT DOCUMENTATION PAGE		Form Approved OMB No. 0704-0188
Public reporting burden for this collection of information is estimated to average 1 hour per response, including the time fo r reviewing instructions, searching existing data sources, gathering and maintaining the data needed, and completing and reviewing the collection of information. Send comments regarding this burden estimate or any other aspect of this collection of information, including suggestions for reducing this burden to Washington Headquarters Services, Directorate for Information Operations and Reports, 1215 Jefferson Davis Highway, Suit 1204, Arlington VA 22202-4302, and to the Office of Management and Budget, Paperwork Reduction Report (0704-0188), Washington DC 20503.		
1. AGENCY USE ONLY *(Leave Blank)*	**2. REPORT DATE**	**3. REPORT TYPE AND DATES COVERED** Final
4. TITLE AND SUBTITLE Novel Cylindrical Cross-Flow Hollow Fiber Membrane Module for Direct Contact Membrane Distillation-based Desalination		**5. FUNDING NUMBERS** R12AC80907
6. AUTHOR(S) Kamalesh K. Sirkar, Dhananjay Singh, Lin Li, Gordana Obuskovic, John Chau		
7. PERFORMING ORGANIZATION NAME(S) AND ADDRESS(ES) New Jersey Institute of Technology Center for Membrane Technologies Room 362 Tiernan Hall 323 Dr. King Blvd Newark, NJ 07102		**8. PERFORMING ORGANIZATION REPORT NUMBER** New Jersey Institute of Technology
9. SPONSORING/MONITORING AGENCY NAME(S) AND ADDRESS(ES) Bureau of Reclamation Denver Federal Center PO Box 25007 Denver CO 80225-0007		**10. SPONSORING/ MONITORING AGENCY REPORT NUMBER**
11. SUPPLEMENTARY NOTES		
12a. DISTRIBUTION/AVAILABILITY STATEMENT		**12b. DISTRIBUTION CODE**

13. ABSTRACT *(Maximum 200 words)*

Direct contact membrane distillation (DCMD) process for recovering water from saline waters appears attractive especially for high salt concentrations if low-cost steam/waste heat is available and waste brine disposal cost for inland desalination is factored in. Although we recently developed successfully a hollow fiber membrane and module with the hot brine in cross- flow over the fibers and obtained high and stable water vapor flux under scaling conditions, the current rectangular membrane module design is unsuitable for larger desalination plants. In the present research, we have developed novel cylindrical cross- flow module containing the high-flux composite hydrophobic hollow fiber membranes at two levels of membrane surface areas: 0.15m^2 and 0.6 m^2. The pipe-like module design is simple, easily scalable, relatively inexpensive, and packs 5 times larger membrane surface area per unit equipment volume compared to the rectangular module design. We have studied distilled water production rates over a feed brine temperature range of 60-91□C. We have developed a model to describe the observed water production rates of such devices in the dead-end brine feed configuration. The model appears to describe well the observed water vapor production rates for different feed brine temperatures at different brine flow rates.

14. SUBJECT TERMS--	**15. NUMBER OF PAGES**
	16. PRICE CODE

17. SECURITY CLASSIFICATION OF REPORT	**18. SECURITY CLASSIFICATION OF THIS PAGE**	**17. SECURITY CLASSIFICATION OF REPORT**	**18. SECURITY CLASSIFICATION OF THIS PAGE**
UL	UL	UL	UL

Desalination and Water Purification Research and Development Program Report No. 175

Novel Cylindrical Cross-Flow Hollow Fiber Membrane Module for Direct Contact Membrane Distillation-based Desalination

Prepared for the Bureau of Reclamation Under Agreement No. R12AC80907
by

Dr. Kamalesh K. Sirkar
Dr. Dhanajay Singh
Ms. Lin Li
Dr. Gordana Obuscovic
Dr. John Chau
New Jersey Institute of Technology Newark, NJ

U.S. Department of the Interior
Bureau of Reclamation
Technical Service Center
Water and Environmental Services Division
Water Treatment Engineering Research Team
Denver, Colorado

October 2013

MISSION STATEMENTS

The U.S. Department of the Interior protects America's natural resources and heritage, honors our cultures and tribal communities, and supplies the energy to power our future.

The mission of the Bureau of Reclamation is to manage, develop, and protect water and related resources in an environmentally and economically sound manner in the interest of the American public.

Disclaimer

The views, analysis, recommendations, and conclusions in this report are those of the authors and do not represent official or unofficial policies or opinions of the United States Government, and the United States takes no position with regard to any findings, conclusions, or recommendations made. As such, mention of trade names or commercial products does not constitute their endorsement by the United States Government.

Acknowledgements

The research conducted under this contract was sponsored by The Desalination and Water Purification Research and Development Program, Bureau of Reclamation, Denver, Colorado.

Contents

Tables

Figures

Page

Acronyms and Abbreviations

AGMD	Air Gap Membrane Distillation
AMT	Applied Membrane Technology Inc.
CFT	central feeder tube
C_p	heat capacity, J/(kg K)
DCMD	Direct Contact Membrane Distillation
d_i	fiber inside diameter, m
d_{ln}	logarithmic mean diameter of fiber, m
d_o	fiber outside diameter, m module
d_s	inside diameter, m central feed tube
d_t	diameter , m
F_c	correction factor in Žukauskas equation
F_d	distillate volumetric flow rate, m^3/h brine
F_f	volumetric flow rate, m^3/h
f_p	fractional packing density of hollow fibers, equation (3) US
gpm	gallon per minute
h_f	shell-side feed heat transfer coefficient, W/(m^2 K)
h_m	membrane heat transfer coefficient, W/(m^2 K)
h_p	tube-side heat transfer coefficient, W/(m^2 K)
ΔH_v	heat of vaporization of water, J/kg
ID	internal diameter
k_m	membrane mass transfer coefficient, kg/(m^2 h Pa)
L	effective fiber length, m
MD	Membrane Distillation
m	number of fiber layers
n_j	fiber number of each layer
N	total fiber number in DCMD module
NJIT	New Jersey Institute of Technology
Nu	Nusselt number
$N_{v,j}$	water vapor flux, kg/(m^2 h) outer
OD	diameter
P PFA	water vapor partial pressure, Pa
PVC	perfluoroalkoxyethylene polyvinyl
PVDF	chloride polyvinylidene fluoride
PP	polypropylene
Pr	Prandtl number
P_{fm}	water vapor partial pressure at the membrane surface on the shell side, Pa
P_{pm}	water vapor partial pressure at the membrane surface on the tube side, Pa
Q	heat transfer rate, W
Re	Reynolds number
SGMD	Sweep Gas Membrane Distillation
T_d	distillate feed temperature, °C
T_f	brine feed temperature, °C
T_{fm}	brine temperature at the membrane surface, °C

T_{pm}	distillate temperature at the membrane surface, °C
u_i	linear velocity on the tube side (fiber lumen), m/s
u_0	interstitial velocity on the shell side, m/s
VMD	Vacuum Membrane Distillation
x	position along the fiber length, m

Greek Letters

ρ	density, kg/m^3
μ	viscosity, Pa s

Subscripts

0	inlet
b	brine
d f	distillate feed
i	inlet
j	the j_{th} fiber layer
m	liquid-vapor interfaces on the brine side and distillate side
o v	brine or shell side vapor
w	wall or membrane surface

Executive summary

Although considerable efforts are being made to improve reverse osmosis technology for desalination, thermally driven membrane distillation is becoming attractive especially for concentrated saline waters having scaling salts. Direct contact membrane distillation (DCMD) studies funded by USBR at NJIT led to the development of novel porous fluorosiloxane-coated porous polypropylene (PP) hollow fibers in a rectangular cross-flow hollow fiber module configuration. In pilot plant studies to concentrate sea water, such a module performed exceptionally well in handling scaling salts present as precipitates as the sea water was concentrated 5.5 times. However the rectangular module designs is complex, the module assembly is very costly and cumbersome and the scale-up possibilities are limited. Further the hollow fiber (HF) packing density is very low.

To overcome such deficiencies, a cylindrical hollow fiber module design was developed where the hot brine would be in cross flow over the porous coated HFs in a radially outward direction from the perforated surface of a central core feeder tube bringing in the hot brine. Further the shell-side spent brine outlet design lacks any shoulder for precipitate accumulation in the shell side. Larger modules were built at Applied Membrane Technology Inc (AMT).

Inc. based on the observed behavior of small modules built at NJIT. The largest AMT module was essentially a very light weight 5.2 cm ID PVC schedule 40 pipe with two end caps and a few threaded outlet pipes providing 0.6 m^2 surface area based on the ID of 1266 coated PP hollow fibers of ID 330μm and OD 630 μm. The membrane surface area per unit equipment volume based on the HF OD is 1526 m^2/m^3. The length of the HFs is 45.7 cm.

The desalination performances of such cylindrical modules having 316 or 1266 HFs were studied in a smaller and a larger setup using a hot brine having 1 wt% salt over 60-91^oC. The performance of the largest module was studied for 18 L/min brine flow rate and brine-in temperatures of 75-80^oC in the larger Direct Contact Membrane Distillation (DCMD) setup. For a distilled water flow rate of 2.5 L/min at a temperature of ~ 25^oC, it was observed that the water vapor flux increased from 7.8 kg/m^2-hr to 14.2 kg/m^2-hr as the brine-in temperature was increased from 76^oC to 79.5^oC.

Of the two modes of operation possible with the brine coming in through the central feeder tube, the performance of the dead-end mode of operation was modeled. Results of water vapor flux obtained via numerical simulation of this mode of operation by solving the governing equations were close to the experimental values. A value of the water vapor mass transfer coefficient close to that obtained in our earlier DCMD studies was the only adjustable parameter. The model simulations predict higher fluxes observed earlier in the rectangular module-based pilot plant studies due to much smaller length of the hollow fibers.

A simple and easily scalable cylindrical module has been developed wherein the hot brine fed by a central core feeder tube is radially flowing across a densely packed set of coated porous hollow fibers through the bore of which distilled water flows for DCMD-based desalination. Such a module may be easily scaled up to shell diameters of 10 to 20 cm; multiple meter^2 membrane surface area can be easily accommodated with very limited possibilities of scaling.

1. Background

The process of Membrane distillation (MD) recovers pure water vapor by passing hot brine on one side of a porous hydrophobic membrane whose pores should remain gas- filled. Direct contact MD (DCMD), vacuum MD (VMD), sweep gas MD (SGMD) and air gap MD (AGMD) (Khayet, 2008) are four different types of MD depending on what happens on the other side of the membrane. In DCMD, cold distillate flows on the other side of the membrane condensing locally the water vapor coming through the pores: the cold distillate gets heated up. This heat is recycled to heat the cooled/spent brine from the DCMD unit in a heat exchanger for further desalination. Some heat from the hot brine is transferred by conduction through the membrane to the cold distillate reducing the process thermal efficiency: less water evaporation takes place.

Considerable amount of work has been carried out throughout the world on the DCMD process (Khayet, 2008). Extensive work has also been carried out in our laboratory to characterize and scale up the DCMD process (Li and Sirkar, 2004; Song et al., 2007; Song et al., 2008) using a novel coated hollow fiber membrane housed in a rectangular cross-flow module as well as develop its cost estimates (Gilron et al., 2007) for desalination and the footprint. The water fluxes achieved were quite high. The membrane performance was stable (Song et al., 2008). This reference describes highly encouraging results from pilot plant studies at around 2.34 L/min (0.62 gallons per minute [gpm]) level of distilled water production using larger modules with funding from USBR. Extensive studies (funded by the US Office of Naval Research) with brines having highly supersaturated solutions of $CaSO_4$ and/or $CaCO_3$ have demonstrated excellent scaling resistance (He et al., 2008; He et al., 2009a; He et al., 2009b) of our porous fluorosiloxane coated polypropylene hollow fiber-based rectangular cross-flow DCMD modules and a countercurrent cascade of modules (Lee et al., 2011). If there is low-cost steam, the technology appears competitive with reverse osmosis (Gilron et al., 2007). Further it can be used to concentrate the brine easily to 20%+ salt (Song et al., 2008) and therefore reduce drastically the cost of brine disposal in inland desalination. Brines having anti-scalants e.g., reverse osmosis concentrates, do not pose any special problem to the membrane in terms of wetting (He et al., 2009b). If waste heat or solar heat sources are available, then the economics gets even better.

The DCMD modules used so far are of the rectangular cross-flow type (Figure 1). Note that figures in this document appear after the main discussion (Section 6).

This figure shows two modules having membrane surface areas of ~ 200 cm^2 and 0.2 m^2. Here hot brine flows on the outside of the hollow fibers in cross flow perpendicular to the picture frame as cold distillate flows through the bores of the hollow fibers. For an energy-efficient process a countercurrent cascade of such cross-flow modules is used (Lee et al., 2011) (Figure 2).The temperature

difference between the hot and cold streams in the countercurrent arrangement is low; the larger the number of cross-flow stages, the lower is the temperature difference. Using a countercurrent cascade, we have experimentally obtained (Lee et al., 2011) a stage thermal efficiency value approaching 90%. This drastic reduction in conductive heat loss has in effect eliminated one important shortcoming of the DCMD vis-à-vis VMD (Li and Sirkar, 2005).

At this time a number of small-scale DCMD demonstrations and commercialization activities are being planned between New Jersey Institute of Technology (NJIT) and other organizations.

The preliminary results from one such activity with Chevron Corporation are available in Singh et al. (2013); this one involved de-oiled produced water sent to NJIT in 55 gallon drums by Chevron Corporation. Currently many steps are involved in treating such a de-oiled water via reverse osmosis including substantial cooling (see Webb et al., 2009 for a detailed process configuration). Our DCMD tests achieved as much as 80% water recovery from such produced water in one step via DCMD; no cooling of the produced water is needed. Chevron Corporation is now planning to build a pilot plant (Chevron, 2014). However, the current rectangular module design appears to create a bottleneck for larger-scale development as described below.

Consider Figure 3 which illustrates the rectangular membrane module structure in greater detail for the smaller membrane module of Figure 1. Part c of this figure shows an assembled module incorporating the picture frame containing the hollow fiber membranes in the middle. On each side of this picture frame we have two separate plastic pieces: the face box (Part a) and the face plate (Part b).The face box is a rectangular thick plastic plate having a central hole for brine inlet or exit. In addition, there is an expanding machined curved surface to distribute the incoming or outgoing flow. The face plate is a thin plate with a very large number of holes drilled in the cross-sectional area for hot brine flow. The diameters of the holes are much smaller in the central flow region corresponding to the brine inlet connection and become progressively larger as we move toward the side walls. The purpose of such a design was to impose a much greater resistance to brine flow in the central region and less resistance in the regions closer to the wall to compensate for brine introduction through the central inlet. The net result was that hot brine entered almost uniformly across the whole cross section of the picture frame even though it was coming through a central tube (Song et al., 2008).

A membrane module used in our studies so far then has five rectangular plastic-based flat components—one picture frame containing the hollow fiber membranes, two face boxes and two face plates. To prevent hot brine leakage, there are two rectangular gaskets on each side of the membrane-containing picture frame, one between the face box and the face plate and the second between the face plate and the picture frame containing the hollow fiber

membranes. Leakage is prevented by having several bolts tightening the whole assembly together. In the case of two such membrane-containing picture frames placed back to back, the number of face boxes and face plates per picture frame can be reduced to one each.

Figure 4 illustrates such an assembly of two DCMD modules back-to-back in what is called a single-pair unit configuration. In fact this figure shows what the modules used in the pilot plant (Song et al., 2008) looked like. These were the largest size modules used in our pilot plant studies (Song et al., 2008); each module had ~ 0.67 m^2 membrane surface area (based on the fiber ID) with two of them put back-to-back. The total membrane surface area in the assembly of Figure 4 is ~1.34 m^2. The overall dimensions of this assembly containing two back-to-back modules are 43 cm x 16.5 cm x 17.5 cm occupying a volume of 12410 cm^3. If we calculate the membrane surface area per unit equipment volume based on the fiber OD (630 μm) instead of the fiber ID (330 μm), the total membrane surface area per unit equipment volume comes out to be 394 m^2/m^3.

The assembly of such modules is very demanding/time consuming with so many bolts and nuts for each module increasing the installation costs per module. Reasonably flat surfaces of the rectangular module face boxes, face plates etc. are needed to prevent hot brine leakage. The amount of wasted volume per module is quite high. Inside each picture frame half of the volume is wasted since the hollow fibers cannot be potted over the whole thickness of the picture frame. Scale up to larger dimensions is highly problematic. In effect, we have to put a very large number of such small units to scale up. Even though it is a hollow fiber-based unit, the effective membrane surface packing density becomes quite low since there is considerable wasted volume inside each module because of the need for fiber potting resulting in a very large footprint and weight in larger-scale plants. Further the cost naturally goes up in a plate and frame configuration due to so many flat plates having well-machined surfaces to provide leak-proof operation, appropriate flow distribution etc.

We have therefore developed a cylindrical cross-flow hollow fiber-based module configuration in this project. This design can resolve such problems and lead to potentially much smoother scale up. This research has investigated the direct contact membrane distillation (DCMD) process for recovering distilled water from saline water using a novel cross-flow hollow fiber membrane module in a cylindrical geometry employing novel membranes studied earlier over the temperature range of ~ 60 to 91^oC

The specific research objectives are:

(1) Develop appropriate cylindrical cross-flow modules of novel coated hydrophobic hollow fibers for the DCMD process.

(2) Investigate the DCMD performances of such membrane modules using simple salt solutions and realistic saline waters.

(3) Model DCMD performances of such modules.

(4) Demonstrate improved economic advantages of such modules in DCMD.

This DCMD technology is especially relevant for saline water sources or water sources containing nonvolatile contaminants primarily of an inorganic nature where there is some waste heat available. A potential list of such sources are: (1) Various locations in the west, southwest of the country where solar heat sources are prevalent or feasible; (2) hot water discharges are encountered at plant and process outlets; (3) low quality heat/steam is available; (4) oil drilling activities which discharge large amounts of usually hot saline water called produced water and require steam generation for oil extraction processes; (5) nuclear waste streams containing nonvolatile radioactive contaminants at low levels; (6) nuclear power plant discharges that are significantly warmer than the ambient.

2. Conclusions and recommendations

1. To investigate the effects of the central brine feed tube design on the performances of a cylindrical cross-flow hollow fiber membrane module, three small modules #1, #2, and #3 were fabricated at NJIT for preliminary DCMD experiments using PVDF hollow fibers. Their performances were explored in a smaller DCMD experimental setup with 1% NaCl containing hot feed solution for different temperatures and different brine flow rates.

2. Based on these preliminary investigations of the water vapor flux and the brine side pressure drop among others, a central feed tube design was communicated to AMT Inc. for fabrication of much larger modules containing fluorosiloxane coated large diameter polypropylene hollow fibers. We received two cylindrical cross-flow hollow fiber membrane modules (large module I and large module II) having an effective area of 0.15 m^2 (based on fiber ID) and one larger module (large module III) having an effective area of 0.6 m^2 (based on fiber ID). The membrane surface area per unit device volume based on the fiber OD for the large module III has a high value of 1526 m^2/m^3 which is quite a few times larger than the rectangular cross-flow hollow fiber modules we wish to replace. The fiber packing fraction has a reasonable value of 0.24. Higher fiber packing fractions are possible.

3. The water vapor flux behaviors of the large modules I and II were explored in a smaller DCMD setup with hot brine containing 1% NaCl in the temperature range of 60-91^oC. A water vapor flux of 16.8 kg/m^2-hr was obtained for a brine- in temperature of 91^oC at a brine flow rate of 18 L/min.

4. The DCMD performance of the large module III was explored in the smaller as well as the larger DCMD experimental setup. The performance of this module was studied for a brine flow rate of 18 L/min and brine-in temperature in the range of 75^oC to 80^oC in the larger DCMD setup. Distilled water flow rate was maintained at 2.5 L/min at a temperature of ~ 25^oC. It was observed that the water vapor flux increased from 7.8 kg/m^2-hr to 14.2 kg/m^2-hr as the brine-in temperature was increased from 76^oC to 79.5^oC.

5. We have developed appropriate equations to develop a model for direct contact membrane distillation carried out in such a cylindrical cross-flow hollow fiber module having a central feed tube for the hot brine. The model was developed for the dead-end brine distribution mode. Simulation results from a numerical solution of these equations describe the observed water vapor flux reasonably well for the dead-end mode of operation. There is only one adjustable parameter here namely, the mass transfer coefficient of the hollow fiber membrane wall.

6. The length of the hollow fibers in the large modules is 45.7 cm which is around two times longer than that used in the largest rectangular cross-flow modules used in previous pilot plant studies. Correspondingly we have lower flux. The model simulations were able to explain this reduction in water vapor flux as a function of increasing length. The model may be used to optimize the module design for further module scale-up.

7. The shell side of these modules was made of PVC; it did show some tendency to deform at higher temperatures ~ 90^{o}C. A material having a somewhat higher temperature–resistance so that it can easily handle at least 90^{o}C is recommended for the shell material.

8. If the brine feed has suspended material including precipitates of scaling salts, a very large part of such material is likely to be deposited on the interior surface of the central feed tube. Periodic cleaning methods will be useful.

9. These newly-developed modules as well as even larger modules should be studied in a pilot plant scale using real-life saline waters.

3. Membrane description and performance

3.1. Membrane modules

A basic design of the cylindrical cross-flow membrane module was developed and the design was communicated to Applied Membrane Technology Inc., Minnetonka, MN (henceforth AMT Inc.). The design is based on our understanding of water vapor transfer rates under particular cross-flow conditions in the larger diameter coated hollow fibers used earlier. The hot brine will be in a radially outward flow configuration through the hollow fiber bed from a central inlet feeder tube. The module design is schematically shown in Figures 5 and 6; AMT Inc. fabricated such type of modules at two levels of membrane surface areas: 0.15 m^2 and 0.6 m^2. Instead of two shell-side outlets at each end of the module, the AMT-fabricated modules had only one outlet. The hollow fibers are porous hydrophobic polypropylene (PP) of internal diameter (ID) 330 μm, wall thickness 150 μm having a pore size of~ 0.6 μm and a porosity of 0.6+ (Membrana, Charlotte, NC). On the outside surface of these hollow fibers there is a light plasma-polymerized fluorosiloxane coating having pores somewhat larger than those of the PP substrate. This was developed by AMT Inc. per our earlier research; it is part of an issued US patent.

Initially a few small modules were fabricated at NJIT using porous hydrophobic polyvinylidene fluoride (PVDF) hollow fibers as a substrate instead of PP; these PVDF fibers were from Arkema Inc., King of Prussia, PA. The performance of these modules (shown in Figure 7) guided the development of the design for the larger modules fabricated at AMT Inc. All the PVDF hollow fiber-based modules were tested at NJIT in a low temperature DCMD set up and subsequently, the changes needed were made to improve the DCMD performances.

The fibers in both types of modules made by AMT Inc. had a length of 45.7 cm (18 inch). The module having lower membrane surface area (Figure 8) had fewer layers of hollow fibers wrapped around a central hot brine inlet tube having holes drilled on their surface for introducing the hot brine feed into the shell side around the hollow fibers. The diameters of such holes increase with distance from the tube inlet(s). The module having a larger membrane surface area has a deeper layer of hollow fibers in the radial brine flow direction to achieve ~ 4 times higher membrane surface area (Figures 9a and 9b). Details of these modules are provided in Table 1. Figure 10 (a, b) illustrates the design and the two o-ring based sealing arrangements at the end of the module with the end caps.

The brine may be introduced in such a module from both ends of the central feeder tube as shown in Figure 5. In such a case, the diameters of the holes on

the wall of the central feeder tube (CFT) increase from both ends toward the middle where the increase in the diameter of the hole stops. On the other hand, if the brine is introduced from one end only as in Figure 6, the diameters of the holes will keep on increasing from the inlet to the other end. Details are provided later.

The shell-side of the modules for DCMD was fabricated from standard size schedule 40 PVC pipe. The end caps for both of the larger size modules (Figure 10) were essentially identical to simplify the potting/tooling at AMT Inc. Standard PVC fittings selected were PVC cemented to the inlet and outlet pipes. Only one shell out pipe at each end was needed as there is an annular space in the module end to collect the flow coming from the shell. The goal was to make a sturdy and light module that will be inexpensive and easy to handle; in addition we wanted much more membrane surface area incorporated in a given volume. Further the module should be capable of being connected to other modules easily. Note: There are no bolts anywhere only a few pipe connections and Phillips screws used to seal the end caps.

There are items in the design which had to be experimentally verified as to how effective they were. One such item is the pressure drop encountered by the shell-side brine as it flows radially outward from the central tube. It depends on the number of holes and the size of the holes on the periphery of the central tube among others. That is why smaller radial cross-flow modules were fabricated in house at NJIT and tested for their DCMD performances. The change in the design of the holes in the central tube as a result of these tests was transmitted to AMT Inc. for changes from preliminary designs. Additional items in the design involve the packing density of fibers, their possibility of oscillation at higher radial flow velocities and the gap at the outer periphery between the fiber bundle and the shell ID.

3.2. Membrane module design and its performance

3.2.1 Design of small membrane modules #1 to #3

In the small membrane module #1, the section having perforated length at the center of the central tube was 15 cm long. The numbers of holes were 122 having a uniform diameter of 0.5 mm. The space (i.e., distance) between two contiguous holes was kept at 0.5 cm. A schematic design of the perforated length of the central tube is shown in Figure 11. As Table 1 indicates, small module #1 fabricated at NJIT had an effective length of 15.6 cm, number of fibers 12, and an effective area of 50.47 cm^2 based on the ID. The details of the PVDF hollow fibers are provided in Table 1. An arrangement was made in the module so that the hot feed solution could enter from both ends of the module.

Based on the experimental results with the small module #1 (described later), another small module (#2) was fabricated at NJIT using the same PVDF hollow fibers by modifying the design of the central tube. Instead of the same sized holes in the central tube, two different sizes of holes were created with the larger holes in the middle part of perforated length and the smaller holes on each side of the larger holes region. The idea behind this was to reduce the pressure drop encountered by the shell-side brine. The modified design of the central tube had 18 large holes of diameter 1 mm in the middle part of perforated length and 52 small holes of diameter 0.5 mm on each side of the larger holes region. The space between two contiguous holes was 0.5 cm. The central tube of both modules #1 and #2 was made at NJIT with perfluoroalkoxyethylene (PFA) tubing. A schematic diagram of the perforated central tube for small module #2 is shown in Figure 12. This module had 15 PVDF porous hollow fibers as before. The length of the module was 15.5 cm; the effective area was 50.47 cm^2 based on ID.

Based on the experimental results from the small membrane module #2, another small membrane module (#3) was fabricated at NJIT using PVDF hollow fibers by modifying the design of the central tube. The sizes of the holes in the perforated length of the middle part of module #3 were larger than those in module #2. The modified design of the central tube had 18 large holes of diameter 2 mm in the middle part of the perforated length and 52 small holes of diameter 1.0 mm on each side of the region having larger holes. The space between two contiguous holes was 0.5 cm. The central tube was made at NJIT with PFA tubing. A schematic diagram of the perforated central tube for module #3 is shown in Figure 13. Further details of this module are provided in Table 1.

3.2.2. Design of large membrane modules I to III

The design of the two large membrane modules I and II received from AMT Inc. will be discussed in some detail. The modules were essentially identical. In large module I, the section having perforated length at the center of the 1.27 cm (0.5 in) diameter central tube was 45.7 cm (18 in) long. The details of the hole numbers and dimensions are provided below. The space between two contiguous holes was kept at around 0.5 cm. A schematic design of the perforated length of the central tube is shown in Figure 14.

The characteristics of the central feeding tube are as follows:

-There are four rows along the tube identified as 1, 2, 3, 4 with equal spacing between them.

-Rows 1 and 3 have a length of 15.24 cm (6.0 in); 5 large holes and 26 smaller holes. Large holes region is at the center of Row 1 and Row 3. Spacing between two holes is 0.508 cm (0.2 in).

-Rows 2 and 4 have length of 14.73 cm (5.8 in); 4 large holes and 26 small

holes. Large holes region is at the center of Row 2 and Row 4. Spacing between two holes is 0.508 cm (0.2 in).

-Total number of small holes = 104; diameter of the small holes = 1 mm

-Total number of large holes = 18; diameter of the large holes = 2 mm.

The large module III received from AMT Inc. had 4 times larger membrane surface area than that of the large modules I and II. This module was fabricated using standard size schedule 40 PVC pipe and has a 2.54 cm (1.0 in) OD perforated central tube in a 5.23 cm (2.06 in) diameter PVC pipe acting as shell. The central tube has 18 large holes and 104 small holes in the middle region of the central tube. Based on preliminary results from the small modules, the design of the central tube was modified. The central tube OD was increased from 1.27 cm (0.5 in) to 2.54 cm (1.0 in) to reduce pressure drop on the shell side. The hole diameters were also modified; now the large holes have a diameter of 6 mm and the small holes 3 mm instead of 2 mm and 1 mm respectively. The number of holes in the central tube was kept the same as in the central tube of the smaller modules. This large module contains 1266 fluorosiloxane coated porous polypropylene hollow fibers with an effective length of 45.7 cm (18 in) and effective membrane surface area of 0.6 m^2 (based on ID). A few photographs of the large module have been shown in Figures 9 and 10.

3.2.3. Experimental setups for DCMD studies

Two experimental setups were used for finding out the DCMD performances of various modules. The smaller experimental setup is shown in a photo in Figure 15a. This setup shown in Figure 15b has been described in detail in Lee et al. (2011); the only difference is that we have only one cylindrical membrane module here and not a countercurrent cascade of four small rectangular cross flow modules. The larger experimental setup shown in Figures 16a and 16b has been described in detail in Song et al. (2007).

3.2.4. DCMD performances of small membrane modules

The small modules #1, #2 and #3 fabricated at NJIT were designed such that the hot feed brine could enter from both ends of the module. Experiments were performed with feed containing 1% NaCl entering from one end or both ends of the module keeping it in horizontal as well as in vertical position. In all experiments, hot brine was passed through the central tube; it radially came out of the central tube to hit porous hollow fibers having cold DI water flowing through them. Due to the very small size of holes in the central feed tube, pressure drop encountered by the shell-side brine was very high. Pressure drop increased from 55.12 kPa (8 psi) to 110.2kPa (16 psi) as the flow rate was increased from 0.8L/min to 1.5 L/min. Water vapor flux increased from 2.4 kg/m^2-hr to 4.2 kg/m^2-hr as the brine temperature was increased from 83^{o}C to

86°C as shown in Figure 17. The water vapor flux is defined as equation 1.

$$Water\ vapor\ flux\ \left(\frac{kg}{m^2-hr}\right)=\frac{Water\ vapor\ collected\ (kg)}{\text{Membrane area based on ID } (m^2) \text{ x time (hr)}} \quad (1)$$

The conductivity on the distillate side was measured using a conductivity meter. It was constant for all experiments indicating no salt leakage from brine side to the distillate side through the membrane.

Experiments with the small module #2 were run with 1% NaCl solution and simulated produced water (synthetic water simulating the composition of the Post WEMCO stream (total dissolved solids, 7622 mg/L) (Singh and Sirkar, 2013)) for different feed temperatures and different flow rates. For 1% NaCl solution at 85°C (Figure 18), water vapor flux increased from 2.3 kg/m^2-hr to 4.2 kg/m^2-hr as brine flow rate was increased from 0.8 L/min to 1.8 L/min. Pressure drop encountered by the shell- side brine was low compared to that in small module #1; it went up from 0 kPa to 89.57 kPa (13 psi) as the brine flow rate was increased from 0.8 L/min to 1.8 L/min. The conductivity on the distillate side was constant for all experiments indicating that there was no salt leakage from the brine side to the distillate side through the membrane.

The performance of the small module #2 was also explored with the simulated de- oiled produced water mentioned above at different temperatures. Water vapor flux increased from 4.2 kg/m^2-hr to 6.6 kg/m^2-hr as the temperature of the produced water was increased from 85°C to 91°C as shown in Figure 19. Water vapor fluxes obtained with the simulated produced water were similar to those obtained with 1% NaCl solution. However, for the simulated produced water, the conductivity on the distillate side was increasing with time for different feed temperatures. After three hours, the conductivity became constant with time irrespective of the feed water temperature. As we had seen in our Chevron-funded project with Chevron-supplied produced water (Singh et al., 2013), the increase in conductivity on the distillate side had probably very little to do with salt leakage or pore wetting. It was primarily due among others to dissolved CO_2 coming to the distillate water from bicarbonates in the feed solution dissociating at the higher temperatures as has been already described in Singh et al. (2013) and He et al. (2009a).

The DCMD performance of the small module #3 was explored for different brine temperatures and different brine flow rates with 1% NaCl solution as feed. As shown in Figure 20, it was found that water vapor flux was as high as 9.9 kg/m^2-hr for a brine temperature of 90°C and a flow rate of 1.8 L/min. Water vapor flux increased from 3.1 kg/m^2-hr to 5.9 kg/m^2-hr as the brine flow rate was increased from 0.8 L/min to 1.8 L/min for the brine temperature of 85°C. Similarly, for a brine temperature of 90°C, water vapor flux increased from 5.3 kg/m^2-hr to 9.9 kg/m^2-hr as the brine flow rate was increased from 0.8 L/min to 1.8 L/min. Due to the modification in the central tube design, pressure drop

encountered by the shell-side brine was much lower compared to those in small module #1 and small module #2; it went up from 0 kPa to 41.34 kPa (6 psi) as the brine flow rate was increased from 0.8 L/min to 1.8 L/min.

3.2.4.1. Effect of the central tube design on the performances of small modules

The design of the central tube was important for the pressure drop encountered by the hot brine on the shell side. Although we have already discussed the specifications of the central tube design for the three small modules, it is useful to summarize them as shown in Table 2. In the small module #1, there were 122 holes in the 15 cm length of the perforated area at the middle of the central tube. All the holes were of uniform diameter of 0.5 mm and spaced at a distance of 0.5 cm. Because of the small diameter of the holes, pressure drop encountered by the shell side brine was quite high, 110.24 kPa (16 psi), for a brine flow rate of 1.5 L/min. High pressure drop is not desirable for an energy-efficient process and forced us to make necessary changes in the module.

In the small module #2, holes were of two different sizes in the perforated region of the central tube of the module; larger holes were at the center and smaller holes were on each side of the larger holes. The modified central tube in the small module #2 resulted in a lower pressure drop encountered by the shell side brine compared to that in small module #1. This result prompted us to increase further the size of the holes in the central tube for small module #3. This design resulted in an even lower pressure drop encountered by the shell side brine compared to that encountered in the small module #2. For the highest brine flow rate of 1.8 L/min studied, the pressure drop was around 41.34 kPa (6 psi). The pressure drop in the larger modules made by AMT Inc. went down further by having a larger diameter of the central tube itself. Figure 21 clearly illustrates the decreasing shell-side pressure drop encountered by the feed brine as the design evolved with the three smaller membrane modules developed at NJIT.

3.2.5. DCMD performances of large membrane modules

Initially two larger modules (I & II) procured from AMT Inc. were tested in the small DCMD setup for low brine flow rates to explore the mode of brine introduction. The identification number of both modules is: EXCT1MDSH SN001. Two module configurations were tested in so far as brine introduction is concerned. In the first configuration called the Dead-End Mode, hot brine comes in through the bore of the 1.27 cm (0.5 in) diameter central distribution tube, goes out radially through the holes in the wall to flow radially across the porous hollow fibers and out. The other end of the central distribution tube is closed. The next configuration is called the Spilt-Flow Mode. In this mode of operation, we utilize the arrangement present in both modules for hot brine introduction from both ends of the central distribution tube. Generally the large module I was operated in the Dead-End Mode and large module II was operated in the Spilt-Flow Mode. We report here results when hot brine containing 1wt%

NaCl was introduced as the feed and deionized water was introduced as the distillate stream.

Figure 22 illustrates the water vapor flux level over a range of brine flow rates going all the way up to 7 L/min. Very limited data were taken at very high brine flow rates. The brine inlet temperature was around 66^{o}C and the distillate (DI water) was coming in at 23^{o}C in a countercurrent fashion through the hollow fiber bore (except for two data points with Module II in Split-Flow Mode). The highest water flux level reached was around 9 kg/m^2-hr. Figure 23 illustrates the variation in the flux for a very minor variation in low brine flow rate for two values of the hot brine temperature for a distillate- in temperature of 25^{o}C for Module I in Dead-End Mode. As expected, a lower brine temperature of 57^{o}C at a low hot brine flow rate of around 335 cm^3/min produces a very low flux level of around 2 kg/m^2-hr; when the hot brine comes in at 74^{o}C, the flux goes up to 4 kg/m^2-hr. For the same hot brine temperature of 74^{o}C and a similar distillate temperature of 21^{o}C, the flux level is almost doubled to 7.2 kg/m^2-hr when the brine flow rate is doubled to 835cm^3/min (Figure 24). Figure 25 illustrates a few more results with both modules for a few values of the hot brine flow rate. It appears that higher brine flow rates up to 2 L/min did not increase the water vapor flux level beyond 8 kg/m^2-hr; this result reinforces the results shown in Figure 22.

3.2.5.1. Experiments with large modules I and II in Split-Flow Mode

The performances of the large modules I and II were studied in the small DCMD experimental setup shown in Figure 15. All experiments were done in Split-flow Mode where the hot brine containing salt at the level of 1 wt% was introduced from both ends of the central distribution tube. These modules were first studied for a lower brine flow rate of 7.2 L/min in the range of 60-72^{o}C of brine-in temperature. Water vapor flux increased from 8.2 kg/m^2-hr to 10.3 kg/m^2-hr as the brine temperature was increased from 61.8^{o}C to 72^{o}C (Figure 26). Values of water vapor fluxes were the same for both modules.

The effect of brine flow rate on the water vapor flux was also studied for module I at a brine-in temperature of 85^{o}C. Distillate-in temperature was maintained ~ 21^{o}C at a flow rate of 0.9 L/min. Brine-in pressure was varying between 6.89 kPag (1 psig) to 27.56 kPag (4 psig). It is observed from Figure 27 that the flux increased from 12 kg/m^2- hr to 13.8 kg/m^2-hr as the brine flow rate was increased from 5 L/min to 18 L/min. Due to limitations of the experimental set up, brine flow rate could not be increased beyond 18 L/min. The conductivity on the distillate side was monitored during the experiments; it was constant indicating that there was no salt leakage from the brine side to the distillate side through the hollow fiber pores.

Module I was also studied at a high brine flow rate of 18 L/min in the range of 80 to 91^{o}C of brine-in temperature. Distillate-in temperature was maintained ~ 22^{o}C for a flow rate of 0.9 L/min. Water vapor flux increased from 12.5 kg/m^{2}-hr to 16.8 kg/m^{2}-hr as the brine-in temperature was increased from 80.5^{o}C to 91^{o}C as shown in Figure 28. Brine-in pressure was around 27.56 kPag (4 psig) during all experiments at the high brine flow rate of 18 L/min. Average value of the brine Reynolds number on the shell side increased from 470 to 1300 as the brine flow rate was increased from 7.2 L/min to 18 L/min (Figure 29). It is clear that when Reynolds number is calculated based on the outer layers, the value is quite low. Therefore when we increase the membrane surface area in such a module to say 2-4 m^{2}, the applicable Reynolds number will become much lower. Based on this primary study, it was concluded that by changing the design of holes in the central tube, the brine side pressure drop can be substantially reduced.

One aspect needs to be mentioned here. The distillate flow rate was low. As a result the distillate was getting heated up to anywhere between 51-63^{o}C. Consequently the temperature driving forces got reduced quite a bit resulting in significantly lower water vapor fluxes. Higher distillate flow rate will facilitate achievement of much higher water vapor fluxes. It is also expected that with higher brine flow rates, even higher values of water vapor flux can be achieved for these modules. Conductivity was constant on the distillate side during all experiments at high temperature indicating no salt leakage from the brine side to the distillate side.

3.2.5.2. Experiments with the larger module III in the smaller DCMD set up

A photograph of the larger module III having a membrane surface area of 0.6 m^{2} is shown in Figure 9a. The performance of the larger module was studied at a high brine flow rate of 18 L/min for hot brine temperature in the range of 55 ^{o}C to 75^{o}C. Distillate-in temperature was maintained around 35^{o}C at a flow rate of 0.5 L/min. The water vapor flux increased from 1.7 kg/m^{2}-hr to 4.3 kg/m^{2}-hr as the brine-in temperature increased from 57^{o}C to 74.2^{o}C as shown in Figure 30. The distillate flow rate was so low that its temperature at the exit went up to 61^{o}C +. As a result the water vapor flux was very low. The performance of the larger module was also explored for a somewhat higher distillate flow rate of 0.9 L/min coming in at a temperature of ~ 35^{o}C. It is observed from Figure 31 that the water vapor flux increased from 3.9 kg/m^{2}-hr to 6.5 kg/m^{2}-hr as the brine-in temperature was increased from 66.6^{o}C to 77^{o}C. The reason for the very low vapor flux is still the very low flow rate of the distillate which was exiting the hollow fibers at around 54-55^{o}C.

3.2.5.3. Experiments with the larger module III in the larger DCMD experimental set up

Experiments were done with the larger module in the larger experimental setup shown in Figure 16. Figure 32 shows the variation of water vapor flux with the brine coming in at a temperature in the range of 55°C to 70°C. The brine flows through the central tube of the module at a rate of 15 L/min and distilled water flows through the bore of the hollow fibers at a rate of 2.5 L/min. The incoming distilled water temperature was maintained around 25°C. Water vapor flux increased from 1.5 kg/m^2-hr to 6 kg m^2-hr as the brine temperature was increased from 57°C to 69°C. Brine in and brine out pressures in the large module were almost zero. Split-flow Mode was employed.

The performance of the module was also tested for a brine flow rate of 18 L/min and brine-in temperature in the range of 76°C to ~ 80°C. Distilled water flow rate was maintained at 2.5 L/min at a temperature of ~ 25°C. It is observed from Figure 33 that the water vapor flux increased from 7.8 kg/m^2-hr to 14.2 kg/m^2-hr as the brine-in temperature was increased from 76°C to 79.5°C. The brine-in and brine-out pressures were almost zero for the brine flow rate of 18 L/min.

3.2.6. Modeling of DCMD performances of large membrane modules

We have conducted a literature search for modeling a radial cross flow hollow fiber membrane module. The relevant paper from outside our group is: Sengupta et al. (1998); but it simply deals with degassing of water. We have a far more complex problem. We have developed appropriate equations to develop a model for direct contact membrane distillation. These are identified below. First consider the pattern of hollow fibers in circles around the central core tube (red) bringing in the hot brine (Figure 34) which spreads out radially throughout the fiber bundle. In any such fiber bundle, focus on one hollow fiber in one particular layer. The various terms needed for mass and energy balances around one hollow fiber at a local section at a distance of x from the distillate entry point is given below (see the notation under Glossary at the beginning).

Consider now a differential slice of the DCMD module with radius *r* and radial

$$dn_j = \frac{f_p(2\pi r_j dr_j)}{\frac{\pi}{4}d_o^2} = \frac{8 f_p r_j dr_j}{d_o^2} \tag{2a}$$

$$n_j = \frac{4 f_p}{d_o^2} r_j^{\,2} \tag{2b}$$

width *dr* identified as the j^{th} fiber layer. The area of this annulus is approximately $2\pi r\, dr$. The number of hollow fiber dn_j inside this slice is obtained from relations in equations (2a) and (2b) given below:

Therefore in the circle of radius r_j the number of hollow fibers located with their center at radius r_j is n_j. Here f_p is the fractional packing density of N number of hollow fibers (of diameter d_o) in the shell side of diameter d_s (around the central core tube of diameter d_t); it is defined as
As the value of r_j increases, the number of fibers in that layer increases with the square of the radius of the radial location.

3.2.6.1. Mass balance on j_{th} layer with n_j number of hollow fibers

The difference in the distillate mass flow rate in the j_{th} layer of fibers is equal to the difference in brine mass flow rate over the j_{th} layer of hollow fibers (see Figure 35) (Note: Distillate flow is here co-current with brine flow direction in the CFT):

$$N\frac{\pi}{4}d^2$$

$$\int_0^L \left[N_{v,j}(x)\right] n_j \pi d_{\ln} dx = \dot{m}_d\Big|_{x=0} - \dot{m}_d\Big|_{x=L} = \rho(F_{d,out} - F_{d,in})\Big|_j \quad (4)$$

$$= \dot{m}_f\Big|_{j-1} - \dot{m}_f\Big|_j = \rho(F_{f,in} - F_{f,out})\Big|_j \quad (5)$$

Here $d_{\ln}$ is defined as:

$$d_{\ln} = \frac{d_o - d_i}{\ln\left(\frac{d_o}{d_i}\right)} \quad (6)$$

Further $N_{v,j}(x)$ is the water vapor mass flux in the j_{th} layer with n_j number of hollow fiber at any x and k_m is the water vapor mass transfer coefficient through the membrane :

$$N_{v.j}(x) = k_m(P_{fm,j}(x) - P_{pm,j}(x)) \quad (7)$$

Here the water vapor partial pressures $P_{fm,j}(x)$ and $P_{pm,j}(x)$ can be expressed using Antoine equation (Smith et al., 2001):

$$P_{fm,j}(x) = 10^3 \exp\left(16.260 - \frac{3799.89}{T_{fm,j}(x) + 273.15 - 46.8}\right) \quad (8)$$

$$P_{pm,j}(x) = 10^3 \exp\left(16.260 - \frac{3799.89}{T_{pm,j}(x) + 273.15 - 46.8}\right) \quad (9)$$

3.2.6.2. Heat Balance on j_{th} layer with n_j number of hollow fibers

The heat gain rate of distillate equals to the heat loss rate of brine:

$$\int_0^x dQ(x)\Big|_j = C_p\left[\dot{m}_d(x)T_d(x) - \dot{m}_d(0)T_d(0)\right] \quad (10)$$

$$= \frac{1}{x}C_p\int_0^x \left(\left[\dot{m}_f(x)T_f(x)\right]\Big|_{j-1} - \left[\dot{m}_f(x)T_f(x)\right]\Big|_j\right)dx \quad (11)$$

3.2.6.3. Shell side brine heat transfer

$$\left.\frac{dQ(x)}{dx}\right|_j = h_{f,j} n_j \pi d_o \left(T_{fo,j}(x) - T_{fm,j}(x)\right) \tag{12}$$

The heat transfer coefficient $h_{f,j}$ in the brine side could be expressed based on Žukauskas equation (Žukauskas, 1987) for given values of Re_o and Pr_o (Song et al.,2007):

$$Nu_{f,j} = \frac{h_{f,j} d_o}{k_o} = 1.04 Re_o^{0.4} Pr_o^{0.36} \left(\frac{Pr_o}{Pr_w}\right)^{0.25} F_c \quad (Re < 40) \tag{13}$$

$$Nu_{f,j} = \frac{h_{f,j} d_o}{k_o} = 0.71 Re_o^{0.5} Pr_o^{0.36} \left(\frac{Pr_o}{Pr_w}\right)^{0.25} F_c \quad (Re > 40) \tag{14}$$

Where

$$Re_o = \frac{d_o u_{o,j} \rho_o}{\mu_o};\ Pr_o = \frac{C_{po}\mu_o}{k_o};\ Pr_w = \frac{C_{pw}\mu_w}{k_w} \tag{15a}$$

$$u_{o,j} = \frac{F_{f,j}}{3600} \times \frac{1}{\pi d_s L - n_j \pi d_o L} \tag{15b}$$

3.2.6.4. Tube side distillate heat transfer

$$\left.\frac{dQ(x)}{dx}\right|_j = h_p n_j \pi d_i \left(T_{pm,j}(x) - T_{p1,j}(x)\right) \tag{16}$$

The heat transfer coefficient h_p in the distillate side could be expressed based on 'Sieder -Tate' equation (Seider and Tate, 1936):

$$Nu_p = \frac{h_p d_i}{k_i} = 1.86 \left(\frac{d_i}{L}\right)^{0.33} \left(Re_i Pr_i\right)^{0.33} \left(\frac{\mu_i}{\mu_{wi}}\right)^{0.14} \tag{17}$$

$$Re_i = \frac{d_i u_i \rho_i}{\mu_i};\ Pr_i = \frac{C_{pi}\mu_i}{k_i} \tag{18a}$$

$$u_i = \frac{F_d}{3600} \times \frac{1}{\frac{N\pi}{4} d_i^2} \tag{18b}$$

3.2.6.5. Heat transfer across hollow fiber membrane

$$\left.\frac{dQ(x)}{dx}\right|_j = h_m n_j d_{\ln} \left(T_{fm,j}(x) - T_{pm,j}(x)\right) + N_{v,j} n_j \pi d_j \left(\Delta H_v (T_{pm,j}(x) + C_{p,j} T_{pm,j}(x)\right) \tag{19}$$

where

$$N_{v,j} = \frac{\int_0^L \left[N_v(x)\right]_j}{L} \tag{20}$$

From the relations given above, we could get the following:
Given the feed conditions of brine and distillate in the j^{th} layer at any x (i.e., the flow rate and the temperature), the values of $T_{fm,j}$ (x), $T_{pm,j}$ (x), $T_{p1,j}$(x), $N_{v,j}$ (x), and $F_{p1,j}$(x) can be calculated from the equations given above, along with the boundary condition $Q(0)\mid_j = 0$ using MATLAB. This assumes that the heat transfer coefficients on the brine side and the distillate side are known. The values of $T_{f1,j}$(x), $Q(x)\mid_j$, $P_{fm,j}$ (x), $P_{pm,j}$ (x) and F_{bo} (x) could then be solved. A detailed notation section has been provided under Glossary.

$$\dot{m}_f\big|_{j+1}(x) = \dot{m}_f\big|_j(x) - N_{v,j}\, n_j\, \pi d_{in} \tag{21}$$

$$T_f\big|_{j+1}(x) = \frac{\dot{m}_j C_p T_f\big|_j(x) - \left(\frac{dQ}{dx}\right)\Big|_j}{\left(\dot{m}_j - N_{v,j} n_j \pi d_{in}\right) C_p} \tag{22}$$

Simulations of the hollow fiber DCMD module performances in rectangular cross-flow were carried out earlier by Song et al. (2008). Those simulations had only one adjustable parameter namely, k_m, the membrane water vapor mass transfer coefficient; its values are available in Sirkar and Song (2009). In the simulations carried out here, k_m is also the only adjustable parameter. Table 3 lists the values used which are not too far apart from those used by Sirkar and Song (2009). The modeling is carried out using the input values V_{b0}, T_{b0}, V_{d0}, T_{d0}, and the details of the module geometry and fiber dimensions and properties.

3.2.6.6. Comparison of simulation results with experimental results

The model illustrated above was based on the hot brine coming in at one end of the central tube with the operation being in the Dead-End Mode. In Figure 36, the experimental results and the simulation results for the large module III in terms of the water vapor flux are shown as a function of the brine temperature varying over 75.2-84.4℃ in this particular mode of operation i.e., the brine flow rate of 18 L/min was in Dead- End Mode as in the simulation. These data were not shown earlier since almost all of the data acquired earlier was in Split-Flow Mode; the data shown in Figure 36 were acquired in very late stages. Further the distillate flow direction is concurrent with respect to the brine flow direction in the CFT. The distillate coming in at 23.9-24.8^{o}C had a flow rate of 2.5 L/min. It appears that the simulation results are somewhat higher but not too far apart from the observed results. Figure 37 illustrates the corresponding scenario for a lower feed brine flow rate of 15 L/min at slightly lower brine temperatures. Here also the simulation results are somewhat higher than the experimentally observed values but not too far apart. The value of k_m used for the large module III (see Table 3) is close to the value of 0.0028 kg/m^2/h/Pa used by Sirkar and Song (2009).

The Dead-End Mode simulated results were also compared with the experimentally observed performances (Figures 32 and 33) of this large module

III in the Split-Flow Mode. Figure 38 illustrates the comparison for a shell-side brine flow rate of 15 L/min coming in at 58-70 ℃ in Split-Flow Mode whereas Figure 39 provides the comparison with the data at a higher shell-side brine flow rate of 18 L/min in the same mode at a higher inlet temperature of 76-80℃. If we compare the performances of the module in two different feed brine flow configurations at say, around 80^{o}C for a brine flow rate of 18 L/min, we find that the Split-Flow Configuration provides a somewhat higher water vapor flux than the Dead-End Configuration. We do not however observe much of a difference at lower feed brine temperatures. The Split-Flow Configuration does have the possibility of providing a more uniform brine flow distribution on the shell side and therefore a better performance.

It is important to note from these two figures that the simulation results obtained in the dead-end mode are significantly higher than the observed values at lower brine temperatures; however at higher temperatures they appear to be close to the experimental values. One reason for this deviation is that the value of the adjustable parameter k_m is somewhat dependent on the temperature; lower k_m values if used for lower feed brine temperatures will bring the simulation results closer to the experimentally observed values at lower temperatures.

It is useful to explore via simulations in the Dead-End Mode what are the effects of the length of the hollow fibers in such a module. The module we have used has an effective fiber length of 45.7 cm (18 inch). Figure 40 illustrates the values of water vapor flux as a function of the hollow fiber length. Table 6 provides numerical values of a variety of relevant quantities. These calculations show that as the hollow fiber length is reduced, the water vapor flux is increased considerably while the distillate outlet temperature rise is reduced which contributes to an increase in the flux. For a perspective we can compare the simulation results shown in Figure 40 with the performance of rectangular cross-flow modules having a length of 24.1 cm of the hollow fibers used earlier in the pilot plant studies (Song et al., 2008). The simulations of Figure 40 suggest a flux of 24.5 kg/m^2-h; those values are not too far away from pilot plant data for the feed brine temperature range being considered.

Experimental data for the operation of the large module I in the Split-Flow Mode are provided in Figures 41 and 42 for comparison with simulated results. Figure 41 describes the flux variation with variation in the distillate flow rate whereas Figure 42 describes the observed flux as a function of the brine temperature in the lower temperature ranges of 61.8-72.1 ^{o}C. Both sets of data correspond to the Split-Flow Mode of operation of the brine while the simulated results are for Dead-End Flow mode. There appears to be a significant difference between the Dead-End Mode simulation results and the Split-Flow Mode experimental data.

3.2.6.7. Advantages of cylindrical cross-flow modules in DCMD

Compared to 18 bolts and nuts used in the previous generation rectangular modules (see Figure 4), the newly developed cylindrical modules do not require

any bolts and nuts (Figures 9 and 10). We have just a few pipe fittings and a few Phillips screws allowing rapid assembly and a very light weight device. Further the device is quite compact. The hollow fiber membrane surface area packed in the cylindrical module has a reasonable value of 1526 m^2/m^3 based on the fiber OD which is 4-5 times larger than that in the rectangular module depending on whether the surface area is based on the fiber OD or ID. The cylindrical module can be easily scaled up to 10-20 cm shell diameter which will accommodate a few times to more than an order of magnitude higher membrane surface area. Putting a large number of such cylindrical modules together in a countercurrent cascade and for larger production rates should be straightforward. The design of the shell side facilitates automatic sweeping away of any precipitates from scaling salts. We have retained the best features of the rectangular cross-flow modules and eliminated their very cumbersome and costly design features which inhibited scale- up for high production levels.

4. References cited

Chevron Corporation, Richmond, CA; Personal Communication with Evan Hatakeyama, June 16, 2014.

Gilron, J.L., L. Song, K.K. Sirkar, 2007. Design for Cascade of Cross-flow Direct Contact Membrane Distillation, I&EC Res., 46, 2324.

He, F., J. Gilron, H. Lee, L. Song, K.K. Sirkar, 2008. Potential for Scaling by Sparingly Soluble Salts in Cross-flow DCMD, J. Membr. Sci., 311, 68.

He, F., K. K. Sirkar, J. Gilron, 2009a. Studies on Scaling of Membranes in Desalination by Direct Contact Membrane Distillation: $CaCO_3$ and mixed $CaCO_3$/$CaSO_4$ systems, Chem. Eng. Sci., 64, 1844.

He, F., Sirkar, K.K., Gilron, J., 2009b. Effects of Antiscalants to Mitigate Membrane Scaling by Direct Contact Membrane Distillation, J. Membr. Sci., 345, 53.

Khayet, M., 2008. Membrane distillation, in "Advanced Membrane Technology and Applications", N.N. Li, A.G. Fane, W.S.W. Ho, T. Matsuura (Eds.), John Wiley, Hoboken, NJ, Chap 6, 297.

Lee, H., He, F., Song L., Gilron, J., Sirkar, K.K., 2011. Desalination with a Cascade of Cross-flow Hollow Fiber Membrane Distillation Devices Integrated with a Heat Exchanger, AIChE J., 57, 1780.

Li, B., and K.K. Sirkar, 2004. Novel Membrane and Device for Direct Contact Membrane Distillation-based Desalination Process, I&EC Res., 43, 5300.

Li, B., and K. Sirkar, 2005. Novel Membrane and Device for Vacuum Membrane Distillation-based Desalination Process, J. Membr. Sci., 257, 60.

Sengupta, A., P.A. Peterson, B.D. Miller, J. Schneider, C.W. Fulk, Jr. 1998. Large-scale Application of Membrane Contactors for Gas Transfer from or to Ultrapure Water, Separation and Purification Technology, 14, 189.

Sieder, E. N.; Tate, C. E. 1936. Heat Transfer and Pressure Drop of Liquids in Tubes. *Ind. Eng. Chem.*, 28, 1429-1435.

Singh, D., P. Prakash, K.K. Sirkar. 2013. Deoiled Produced Water Treatment using Direct-Contact Membrane Distillation, I&EC Res., 52, 13439.

Kamalesh K. Sirkar, Liming Song. 2009. Pilot-Scale Studies for Direct Contact Membrane Distillation-Based Desalination Process, U.S. Department of the Interior Bureau of Reclamation Desalination and Water Purification Research

and Development Program Report No.134. Online resource: http://www.usbr.gov/research/AMT/reportpdfs/report134.pdf.

Smith, J. M.; Van Ness, H. C.; Abbott, M. M. 2001. *Introduction to Chemical Engineering Thermodynamics*, 6th ed. international ed.; McGraw-Hill Higher Education: New York, pp 328-367.

Song, L., B. Li, K.K. Sirkar, J.L. Gilron, 2007. Direct Contact Membrane Distillation- based Desalination: Novel Membranes, Devices, Larger-scale Studies and a Model, I&EC Res., 46, 2307.

Song, L., Ma, Z., Liao, X., Kosaraju, P. B., Irish, J. R., Sirkar, K. K., 2008. Pilot Plant Studies of Novel Membranes and Devices for Direct Contact Membrane Distillation- based Distillation, J. Membr. Sci., 323, 257.

Webb, C., Nagghappan, LNSP, Smart, G., Hoblitzell, J., Franks, R., 2009. Desalination of Oilfield-Produced Water at the San Ardo Water Reclamation Facility, CA, SPE 121520-PP.

Žukauskas, A. Heat Transfer from Tubes in Cross-flow. 1987. *Adv. Heat Transfer/*, 18, 87- 159.

5. Tables

Table 1.—Details of different membrane modules and hollow fibers

Particulars	Small module #1	Small module #2	Small module #3	Large module I	Large module II	Large module III
Membrane type	PVDF	PVDF	PVDF	Coated PP*	Coated PP*	Coated PP*
Fiber ID (μm)	692	692	692	330	330	330
Fiber OD (μm)	925	925	925	630	630	630
No. of fibers	15	15	15	316	316	1266
Effective fiber length (cm)	15.5	15.5	15.5	45.7	45.7	45.7
Effective membrane surface area (cm^2)**	50.4	50.4	50.4	1500	1500	6000
Fiber packing fraction	N/A	0.03	0.03	0.13	0.13	0.24
Fiber surface area per unit volume (m^2/m^3)***	N/A	N/A	N/A	1120	1120	1526
No. of smaller holes	122	104	104	104	104	104
No. of larger holes	N/A	18	18	18	18	18
Diameter of smaller holes (mm)	0.5	0.5	1.0	1.0	1.0	3.0
Diameter of larger holes (mm)	N/A	1.0	2.0	2.0	2.0	6.0
Space between two holes (mm)	0.5	0.5	0.5	0.5	0.5	1.5
CFT ID (cm)****	0.5	0.5	0.5	1.3	1.3	2.5
Module ID (cm)	N/A	2.0	2.0	2.8	2.8	5.2
Module length (cm)	15.5	15.5	15.5	45.7	45.7	45.7
Fabricated at	NJIT, NJ	NJIT, NJ	NJIT, NJ	AMT Inc., MN	AMT Inc., MN	AMT Inc., MN

* Fluorosiloxane coated; ** Based on fiber inner diameter; *** Based on fiber outer diameter;
**** CFT - Central Feeder Tube

Table 2.—Specifications of the central tubes of different small modules

	Number of Smaller Holes	Number of Larger Holes	Diameter of Smaller Holes	Diameter of Larger Holes	Space Between Two Holes (cm)
Module #1	122	-	0.5	-	0.5
Module #2	104	1	0.5	1	0.5
Module #3	104	1	1.0	2	0.5

Tables

Table 3.—Values of the parameters used in model simulations for Dead-End Mode

Reference Temperature T_0	273.15 K
Liquid water heat capacity, C_p	4.1863 kJ/kg-C
Liquid water density	1 g/cm^3
Latent heat of evaporation	2257 kJ/kg
Thermal conductivity for polypropylene, k_{pp}	0.17 W/m-K
Thermal conductivity for air, k_{air}	0.025 W/m-K
Mass transfer coefficient k_m for large module I	0.0017 kg/m^2/h/Pa
Mass transfer coefficient k_m for large module III	0.0033 kg/m^2/h/Pa

Table 4(a).—Experimental results for Figure 36

T_{bi}	T_{bo}	T_{di}	T_{do}	Flux
°C	°C	°C	°C	kg/m^2-h
75.2	68	24.2	30.8	10.4
77.5	70.4	24.2	31.4	10.7
78.9	71.6	23.9	31.4	11.0
83.1	75.5	24.8	31.9	12.1
84.4	76.1	24.8	32.4	12.3

Table 4(b).—Simulation results for Figure 36

T_{bi}	T_{bo}	T_{di}	T_{do}	Flux
°C	°C	°C	°C	kg/m^2-h
75.2	68.5	24.2	31.1	10.5
77.5	70.5	24.2	31.4	11
78.9	71.6	23.9	31.7	11.3
83.1	75.3	24.8	31.9	12.4
84.4	76.5	24.8	32.2	12.7

Table 5(a).—Experimental results for Figure 37

T_{bi}	T_{bo}	T_{di}	T_{do}	Flux
°C	°C	°C	°C	kg/m^2-h
59.9	55.1	24.1	27.1	4.8
75.5	70.2	25.4	31.3	7.4
79.9	72.0	25.4	31.3	9.8

Table 5(b).—Simulation results for Figure 37

T_{bi}	T_{bo}	T_{di}	T_{do}	Flux
°C	°C	°C	°C	kg/m^2-h
59.9	54.2	24.1	27.6	5.8
75.5	68.3	25.4	31.2	8.9
79.9	72.0	25.4	31.3	9.9

Table 6.—Detailed temperature and flux information for large module III simulations per Figure 40

Fiber length (cm)	Fiber length (inch)	Tbi (°C)	Tbo (°C)	Tdi (°C)	Tdo (°C)	Flux (kg/m2-h)
45.7	18	79.5	74.0	25.2	32.5	14.9
43.2	17	79.5	74.0	25.2	32.2	15.0
40.6	16	79.5	74.1	25.2	31.9	15.7
38.1	15	79.5	74.1	25.2	31.5	16.6
35.6	14	79.5	74.2	25.2	31.1	17.5
33.0	13	79.5	74.3	25.2	30.6	18.7
30.5	12	79.5	74.4	25.2	29.9	19.9
27.9	11	79.5	74.5	25.2	29.1	21.3
25.4	10	79.5	74.6	25.2	28.3	22.8
22.9	9	79.5	74.8	25.2	27.2	24.5
20.3	8	79.5	75.0	25.2	25.8	26.5
17.8	7	79.5	75.2	25.2	24.2	28.7
15.2	6	79.5	75.5	25.2	22.1	31.4

Table 7(a).—Experimental results for Figure 41

T_{bi} (°C)	T_{bo} (°C)	T_{di} (°C)	T_{do} (°C)	F_{bi} (L/min)	F_{di} (ml/min)	Flux (kg/m^2-h)
62.2	56.2	22.8	55.9	5	500	8.3
63.6	57.2	22.5	55.4	5	570	8.4

Table 7(b).—Simulation results for Figure 41

T_{bi} (°C)	T_{bo} (°C)	T_{di} (°C)	T_{do} (°C)	F_{bi} (L/min)	F_{di} (ml/min)	Flux (kg/m^2-h)
62.2	58.7	22.8	57	5	500	13.3
63.6	59.5	22.5	57.7	5	570	15.6

Table 8(a).—Experimental results for Figure 42

Tbi (°C)	Tbo (°C)	Tdi (°C)	Tdo (°C)	Flux (kg/m2-h)
61.8	58.4	23.3	55.6	8.3
65.5	62.2	31.3	59.4	8.5
66.7	63.2	31.5	60.1	9.1
69.4	65.7	35.3	63.3	9.9
72.1	68.6	37.8	67.5	10.1

Tables

Table 8(b).—Experimental results for Figure 42

Tbi	Tbo	Tdi	Tdo	Flux
(℃)	(℃)	(℃)	(℃)	(kg/m2-h)
61.8	59.1	23.3	56.8	14.8
65.5	63.1	31.3	61.1	13.3
66.7	64.2	31.5	62.2	13.8
69.4	67	35.3	65	13.5
72.1	68.6	37.8	67.7	13.7

Table 9.—Experimental results for Figure 28

Tbi	Tbo	Tdi	Tdo	Flux
(℃)	(℃)	(℃)	(℃)	(kg/m2-h)
80.5	79	21	70.8	12.5
85.5	84	21.4	77.5	13.8
87.2	85.5	21.1	76.3	14.6
89	87.2	21.7	78.5	15.2
90	88.1	22.3	77.4	15.9
91	89.1	18	75.2	16.8

Table 10(a).—Experimental data for Figure 38

Tbi	Tbo	Tdi	Tdo	Flux
℃	℃	℃	℃	kg/m2-h
57.5	54	23	29.4	1.5
60.2	56.4	23.8	30.5	3
62.2	56.4	23.9	31.5	3.4
64	60	24.3	32.1	4
65	60.7	24.3	32.6	4.5
65.8	61.4	24.3	33.2	4.8
68.5	63.4	24.5	33.8	5.5
69.4	64.4	25	33.6	6.1

Table 10(b).—Simulation results for Figure 38

Tbi	Tbo	Tdi	Tdo	Fbi	Fdi	Flux
℃	℃	℃	℃	L/min	L/min	kg/m2-h
57.5	53.9	23	29.1	15	2.5	5.3
60.2	56.3	23.8	31.6	15	2.5	5.8
62.2	58	23.9	33.3	15	2.5	6.2
64	59.7	24.3	34.9	15	2.5	6.6
65	60.6	24.3	35.7	15	2.5	6.8
65.8	61.3	24.3	36.4	15	2.5	7.0
68.5	63.7	24.5	38.7	15	2.5	7.5
69.4	64.6	25	39.5	15	2.5	7.7

Table 11(a).—Experimental data for Figure 39

Tbi	**Tbo**	**Tdi**	**Tdo**	**Flux**
(℃)	**(℃)**	**(℃)**	**(℃)**	**(kg/m2-h)**
76	72.2	26.4	38.1	7.8
76.6	72.4	25	38.2	9
77.2	72.9	24.3	38	11.6
78	73.8	26.4	39	12.6
78.8	74.5	26	39.4	13.4
79.5	75.3	25.2	39.4	14.2

Table 11(b). Simulation results for Figure 39

T_{bi}	T_{bo}	T_{di}	T_{do}	F_{bi}	F_{di}	Flux
℃	℃	℃	℃	L/min	L/min	kg/m^2-h
76	71.6	26.4	35.9	18	2.5	10.7
76.6	72	25	36.1	18	2.5	10.8
77.2	72.5	24.3	36.5	18	2.5	10.9
78	73.4	26.4	37.6	18	2.5	11.1
78.8	74	26	38.2	18	2.5	11.3
79.5	74.6	25.2	38.6	18	2.5	11.5

6. Figures

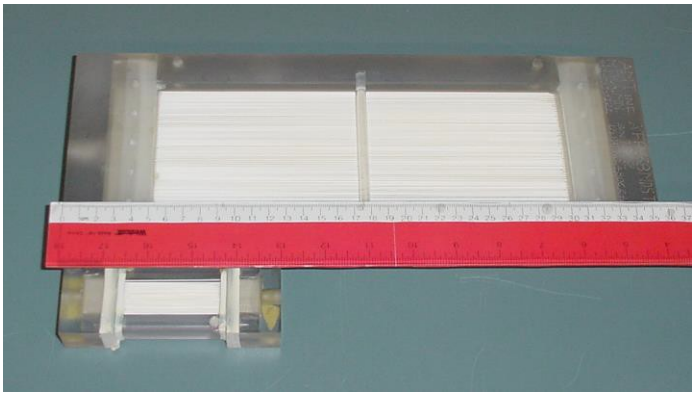

Figure 1.—Photo of small size membrane module and larger size module used with a scale in between (the cover plate and the flow distributor plates have not been shown)(Song et al., 2007).

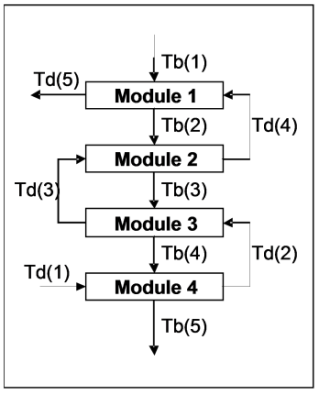

Figure 2.—Scheme for cross-flow DCMD modules in a countercurrent cascade: hot brine is in cross flow over the fibers; cold distillate moves through the fibers from low to high temperature (Lee et al., 2011).

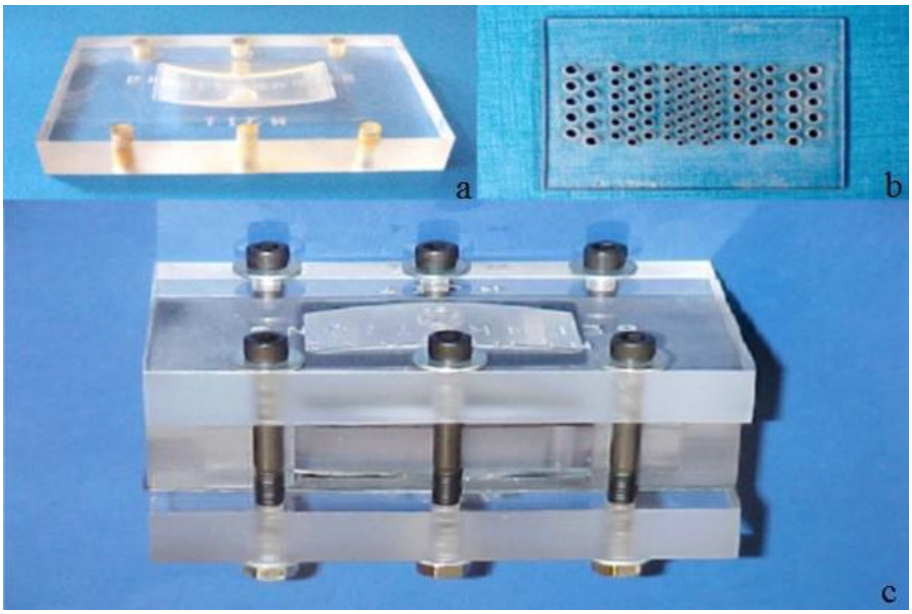

Figure 3.—a) Face box fabricated for a small rectangular cross flow module; b) Face plate fabricated for rectangular cross flow module; c) Rectangular cross flow test module with face boxes, face plates and assembly.

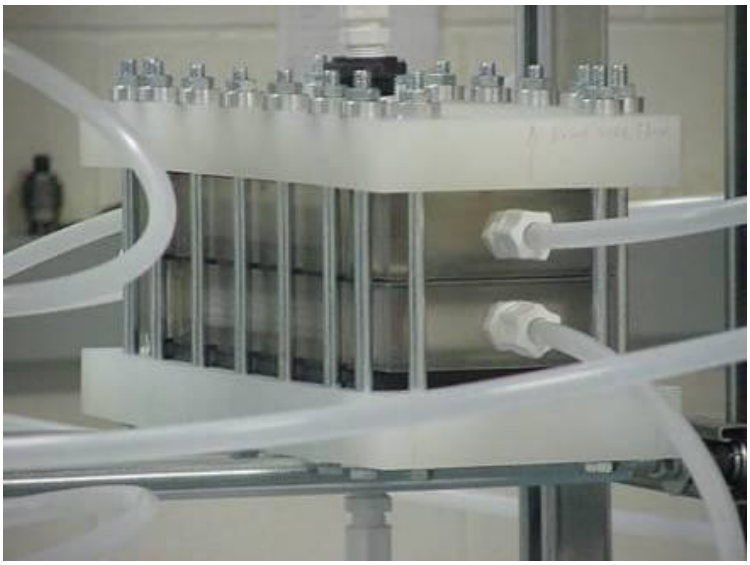

Figure 4.—Photo of two rectangular DCMD modules back-to-back in the single-pair unit configuration in the pilot plant set-up (Song et al., 2008).

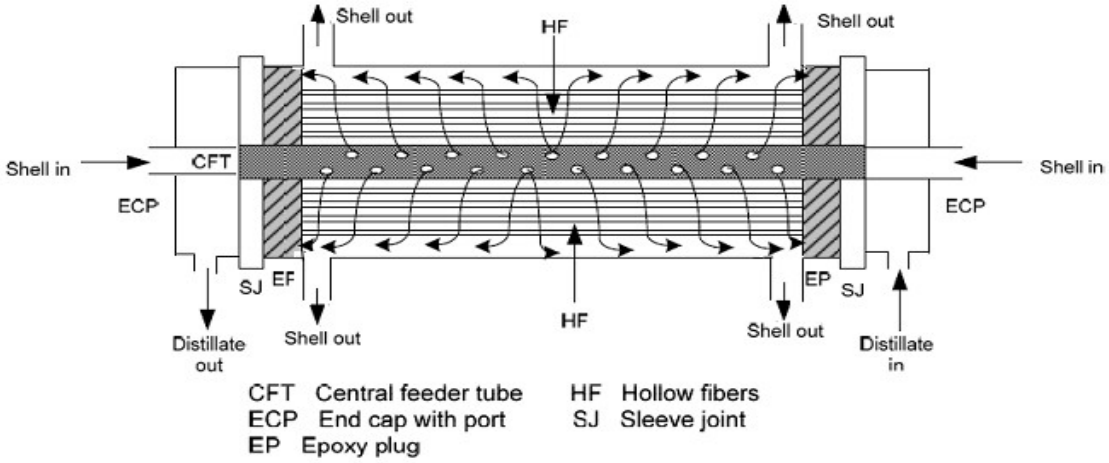

Figure 5.—Schematic view of cross-flow module with flow directions at the shell side and feed brine entering the central feeder tube from both sides.

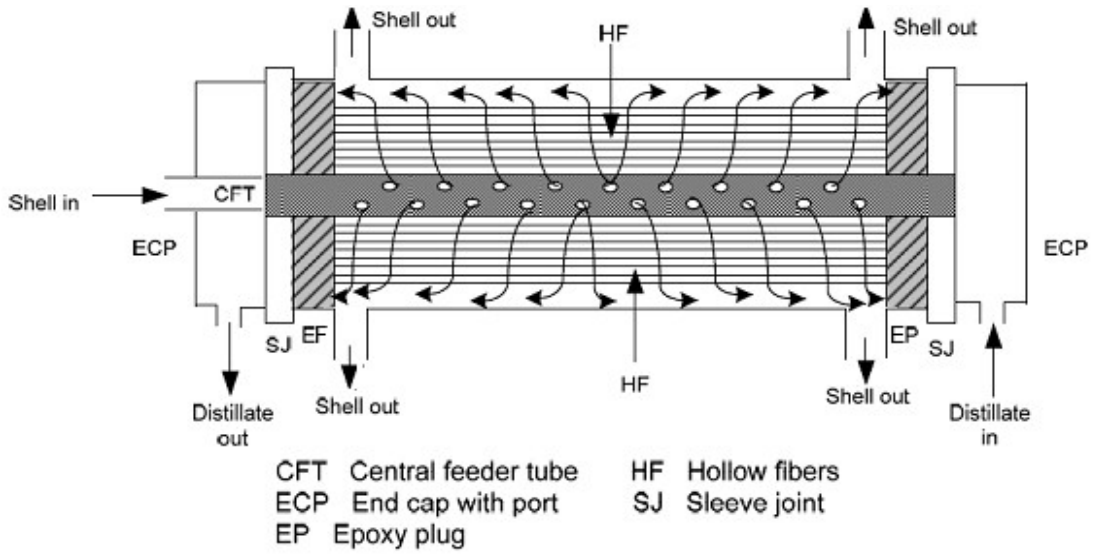

Figure 6.—Schematic view of cross-flow module with flow directions at the shell side and feed brine entering the central feeder tube from one side only.

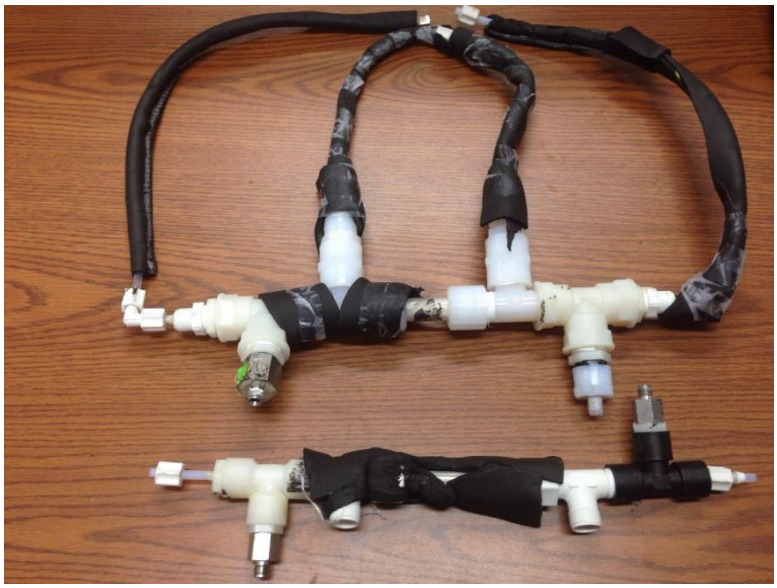

Figure 7.—Photo of two of the small modules fabricated at NJIT using PVDF hollow fibers for testing the designs of the central feed inlet tube.

Figure 8.—Photo of two AMT-fabricated large modules I and II.

(a)

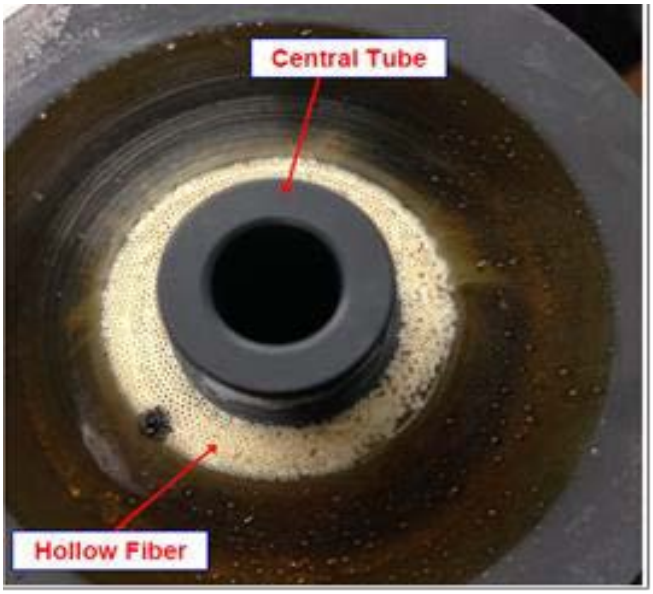

(b)

Figure 9.—Photographs of (a) the large module III received from AMT, Inc. and (b) the cross- sectional view of the large module III showing the central tube and the ends of the PP hollow fibers.

(a) (b)

Figure 10.—Photos of Inside of End Sections of Large AMT Module III (a) & (b): Two O-Rings; Large O-Ring sealing the End Cap; Small O-Ring sealing the Central Brine Feed Tube.

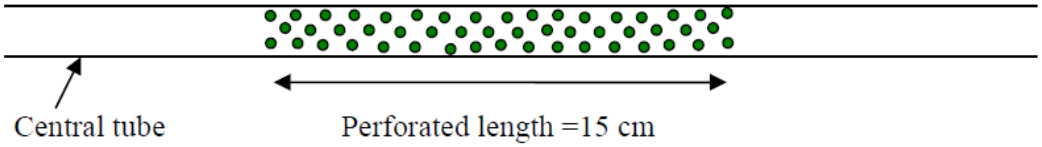

Figure 11.—Schematic design of the central tube for small module #1 having a perforated length of 15 cm in the middle part of tube.

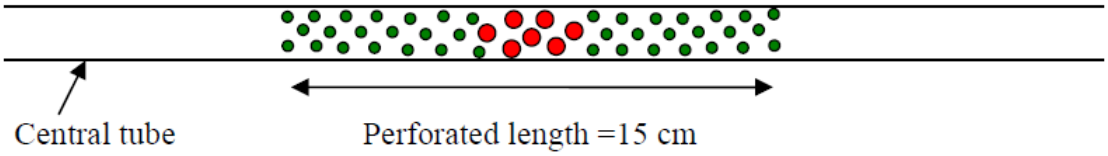

Figure 12.—Schematic design of the central tube for small module #2 having perforated length of 15 cm in the middle part of tube. The holes are larger at the center and smaller on each side of the region containing larger holes.

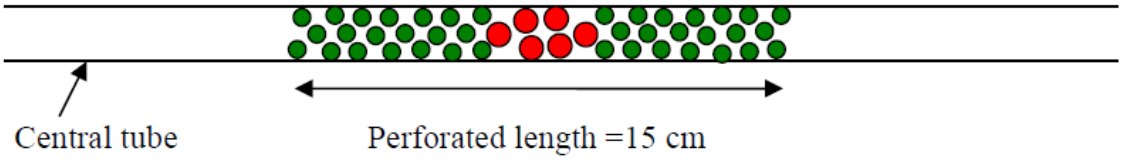

Figure 13.—Schematic design of the central tube for small module #3 having a perforated length of 15 cm in the middle part of tube. The holes are larger at the center and smaller at both ends of the region containing larger holes.

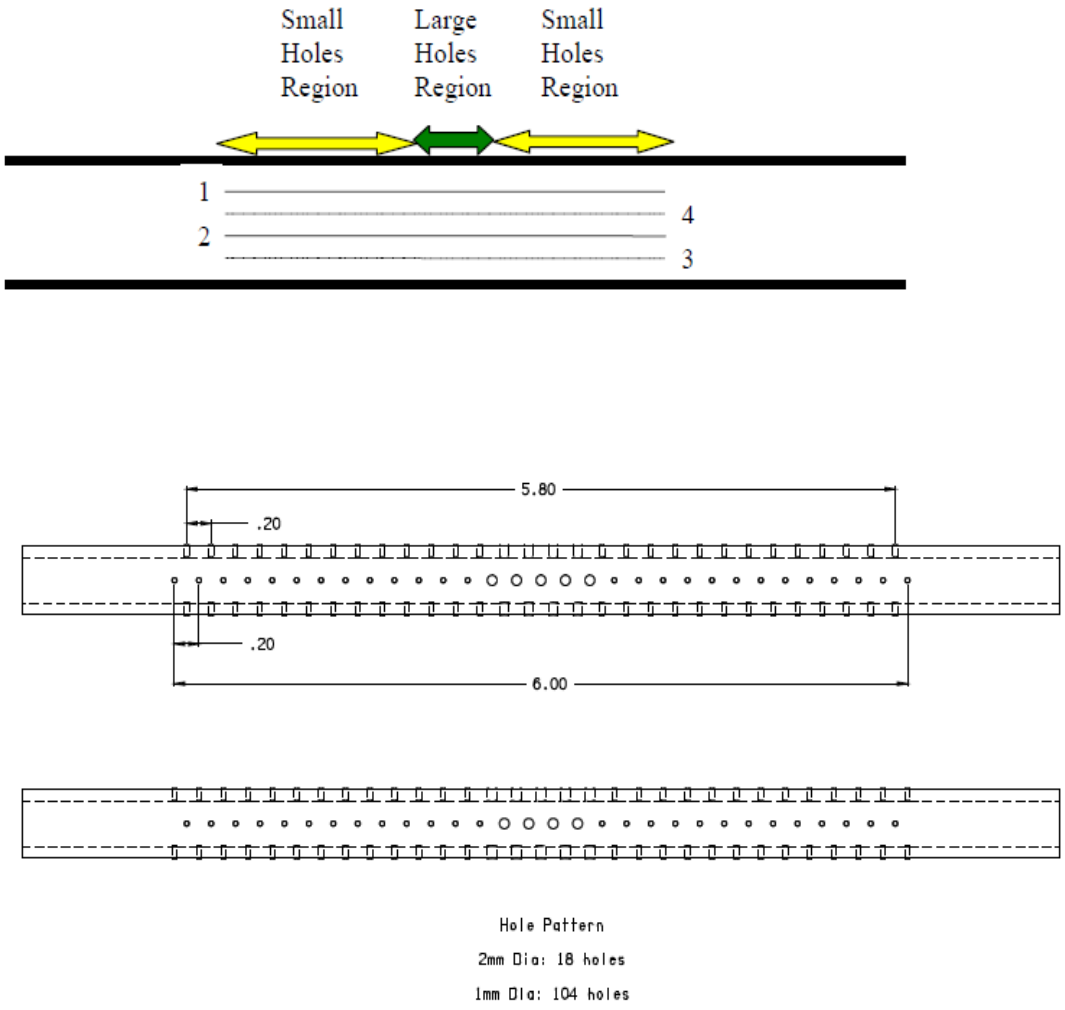

Figure 14.—Schematic design of the central tube for AMT-fabricated large module I or module II having a perforated length of 15.24 cm (6 in) in the middle part of tube.

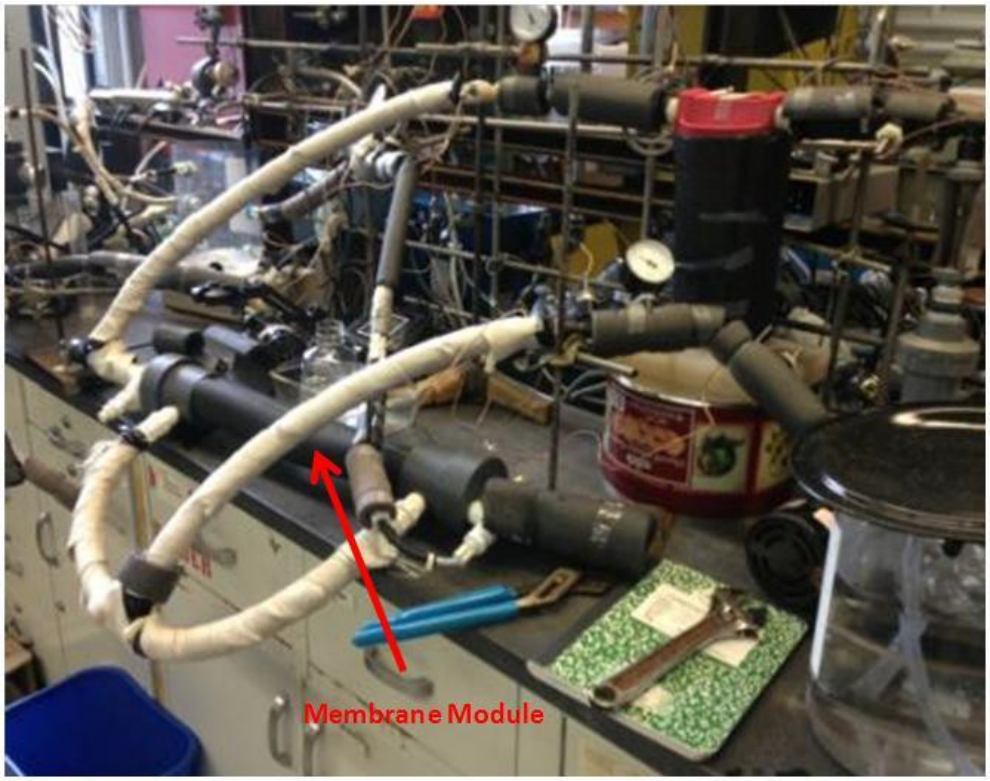

Figure 15a.—Photograph of the smaller DCMD experimental setup.

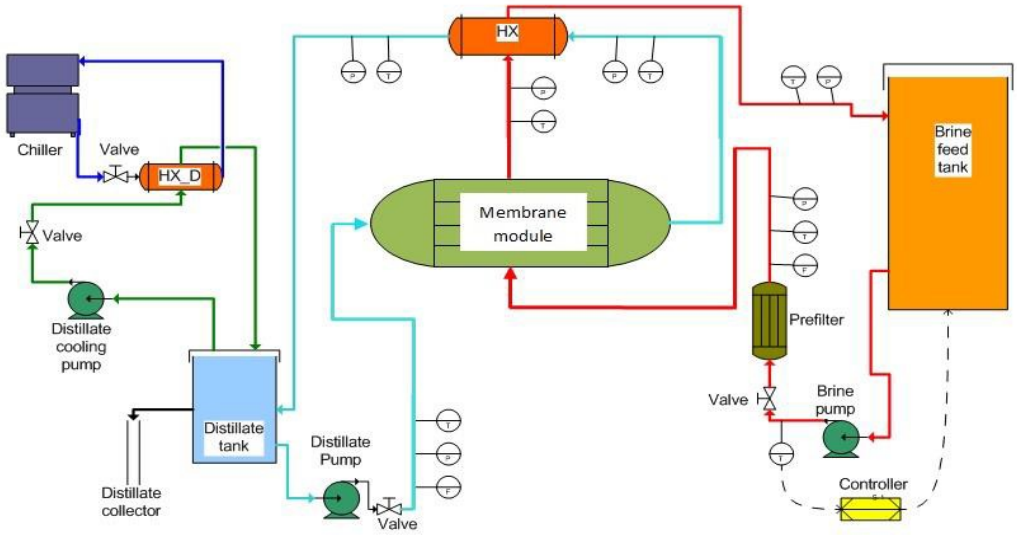

Figure15b.—Schematic diagram of the smaller experimental setup for DCMD with a heat exchanger (HX) and a membrane module (Modified from Lee et al., 2011).

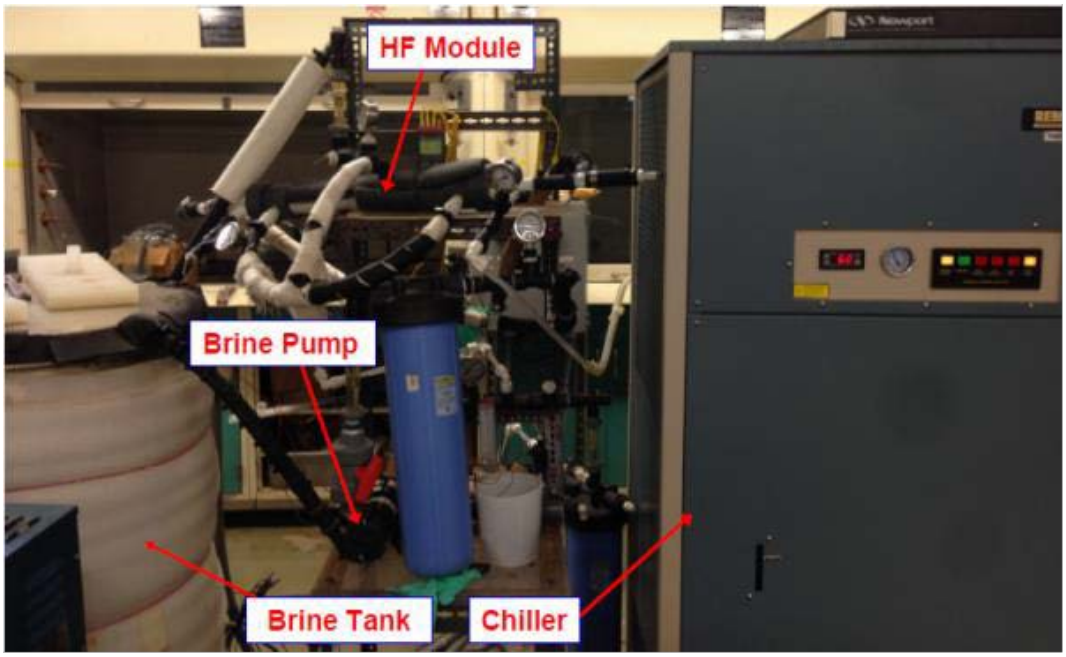

Figure 16a.—Photograph of the larger DCMD experimental setup.

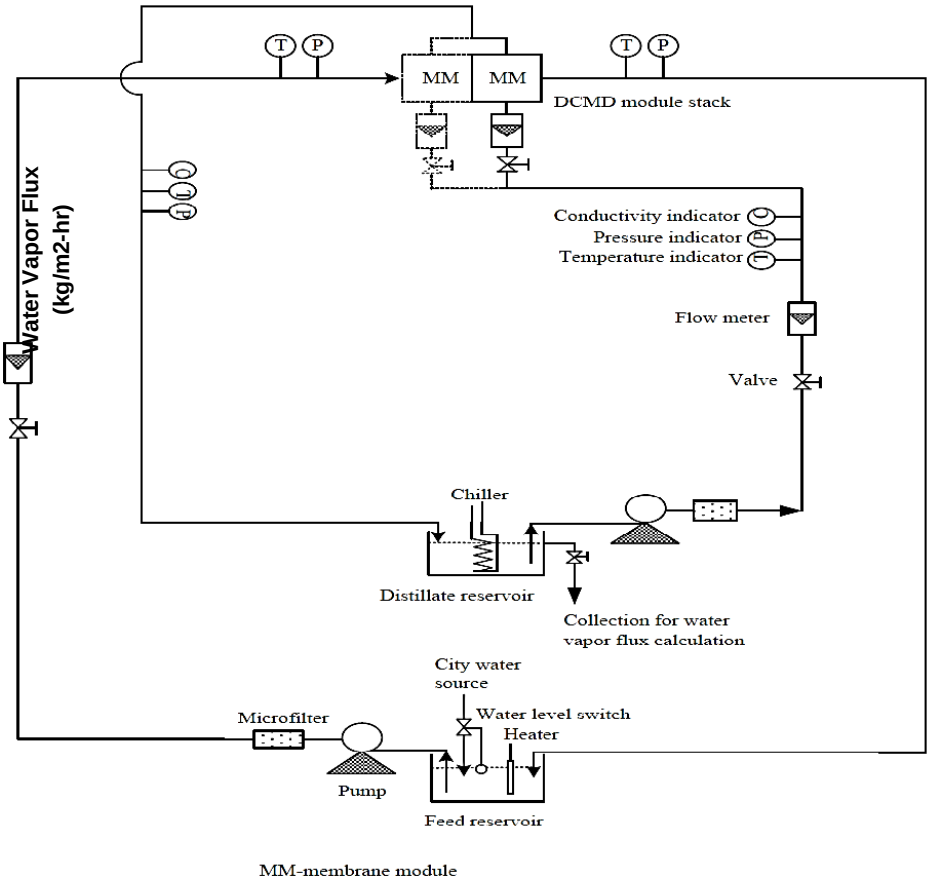

Figure 16b.—Process flow diagram for the larger DCMD experimental setup (Song et al., 2007).

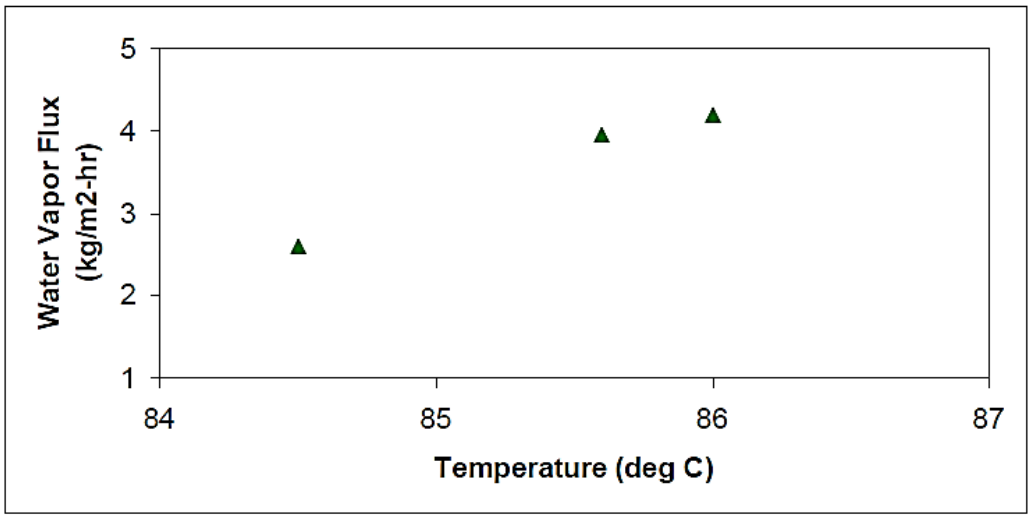

Figure 17.—Change in water vapor flux with temperature in PVDF hollow fiber containing small module #1; distillate in temperature ~20°C.

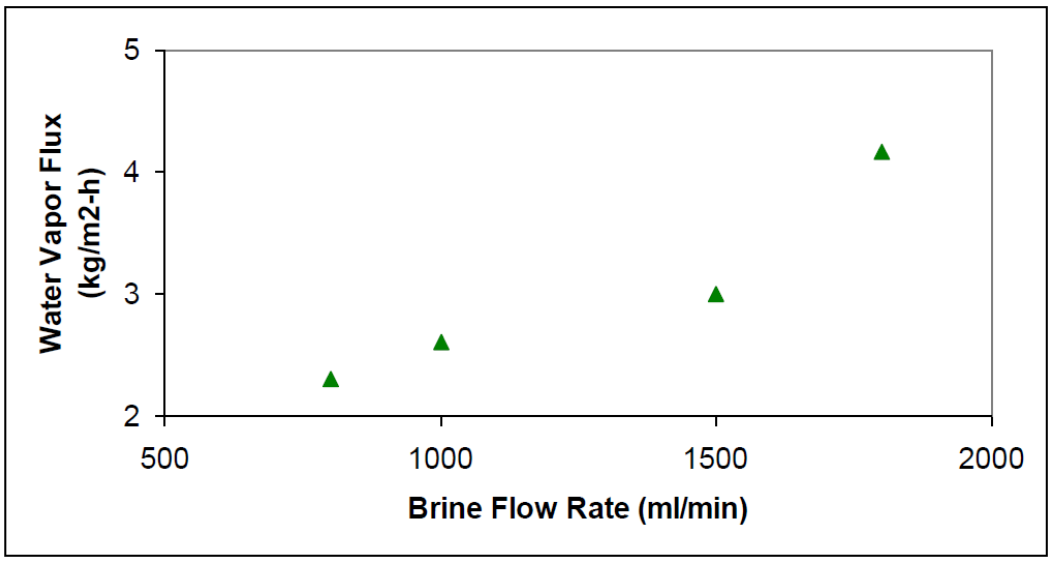

Figure 18.—Change in water vapor flux with different flow rates of 1% NaCl solution at 85°C in small module #2; distillate in temperature ~20°C.

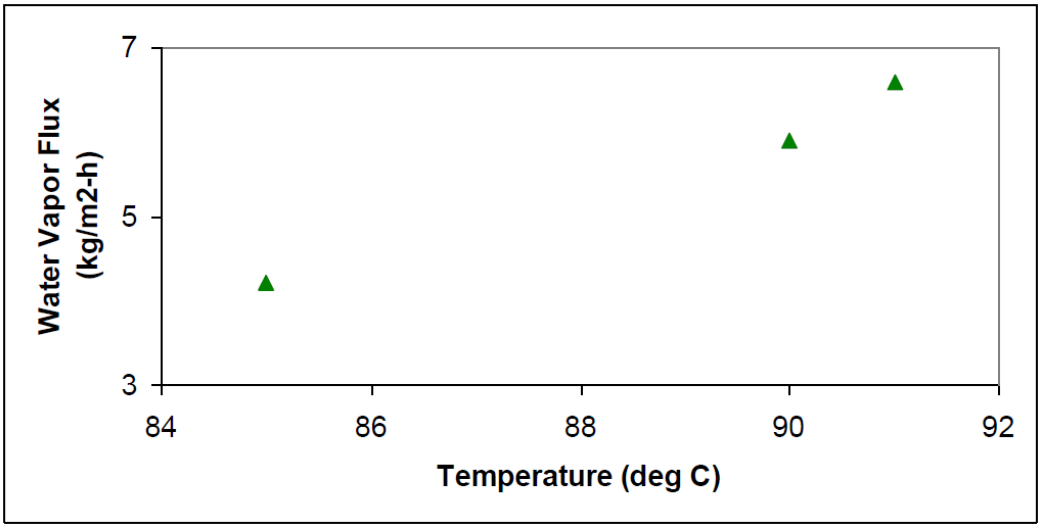

Figure 19.—Change in water vapor flux with temperature of a simulated de-oiled produced water in small module #2 for a simulated produced water flow rate of 1800 ml/min; distillate in temperature ~20°C.

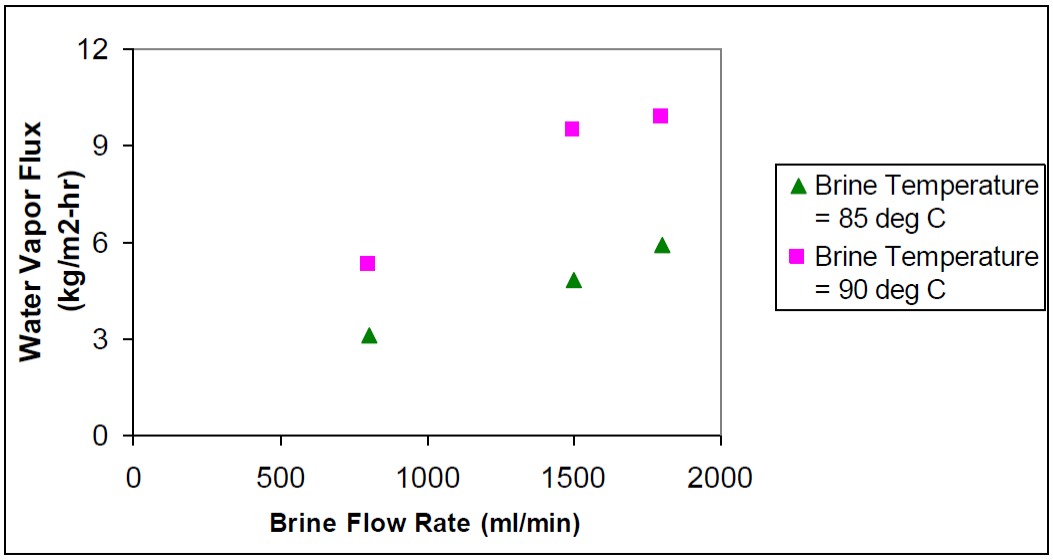

Figure 20.—Change in water vapor flux with different brine flow rates for 1% NaCl solution at different temperatures in small module #3; distillate in temperature ~20°C.

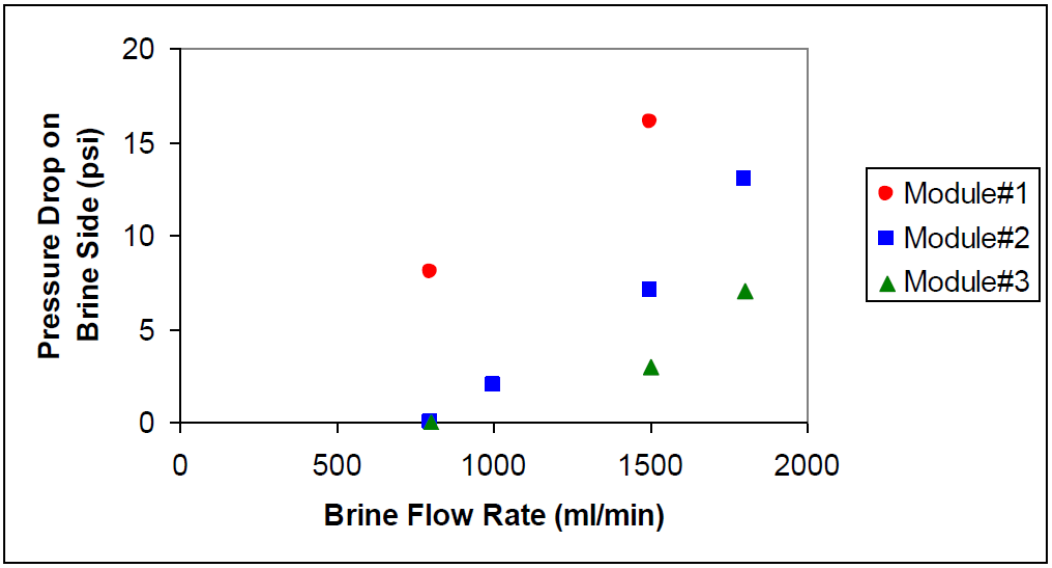

Figure 21.—Change in pressure drop encountered by shell side brine for different brine flow rates for small modules #1, #2 and #3.

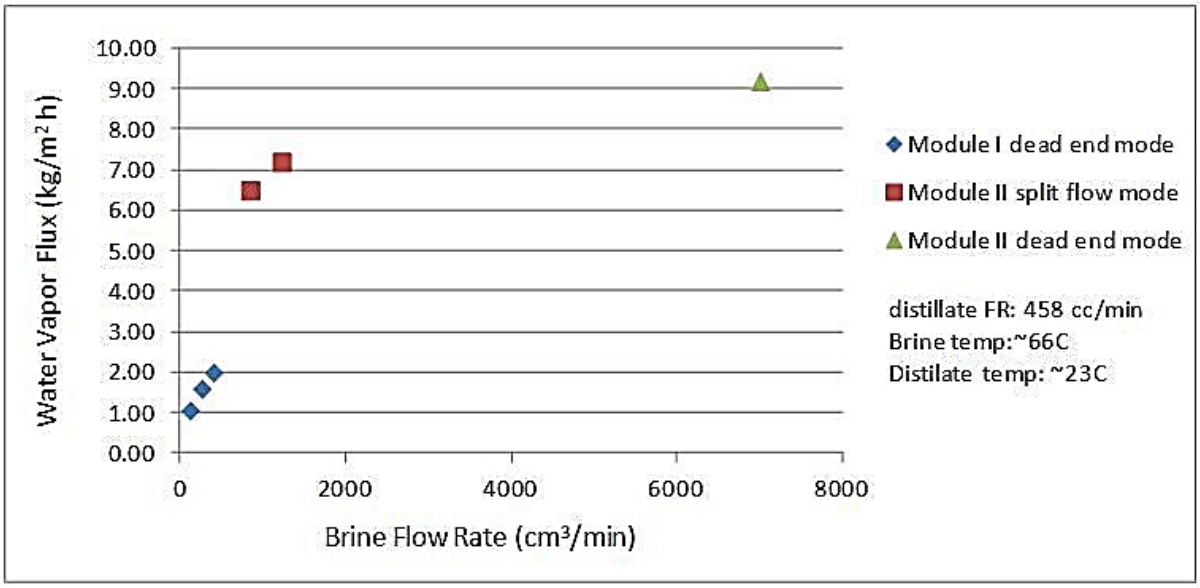

Figure 22.—Change in water vapor flux with different flow rates of 1% NaCl solution at 66°C in large Module I and large Module II for different flow patterns; average distillate in temperature ~23°C.

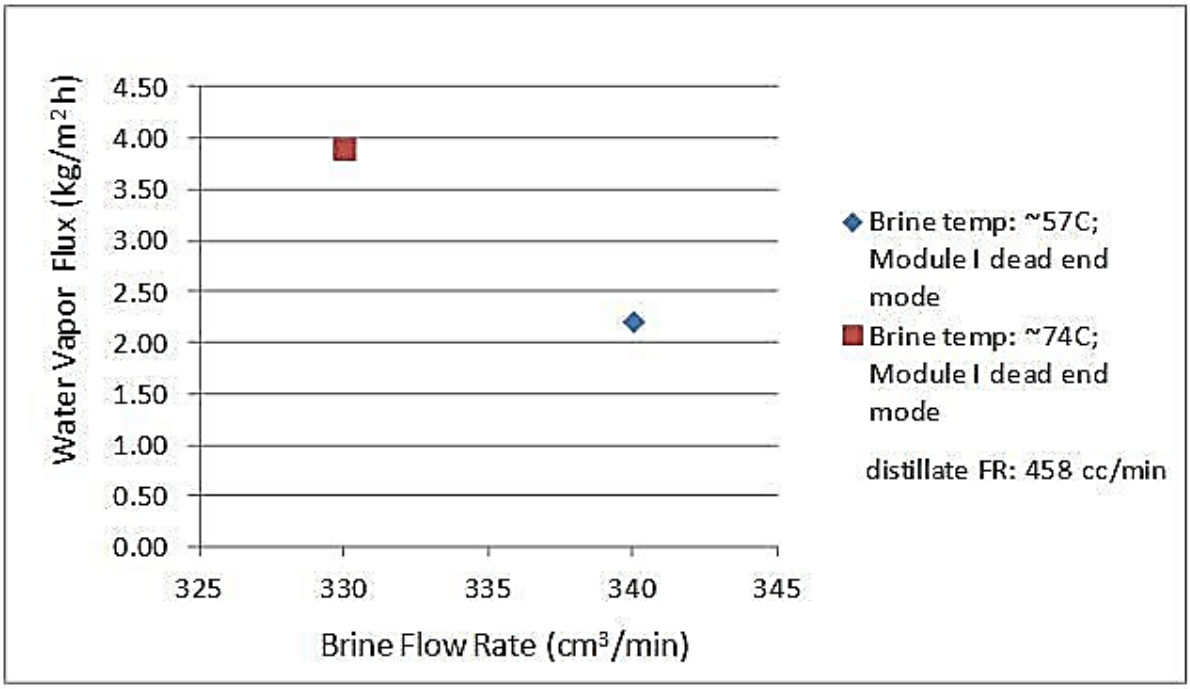

Figure 23.—Change in water vapor flux with temperature using large module I (Dead-End Mode) for a similar brine flow rate: average distillate temperature ~25 °C.

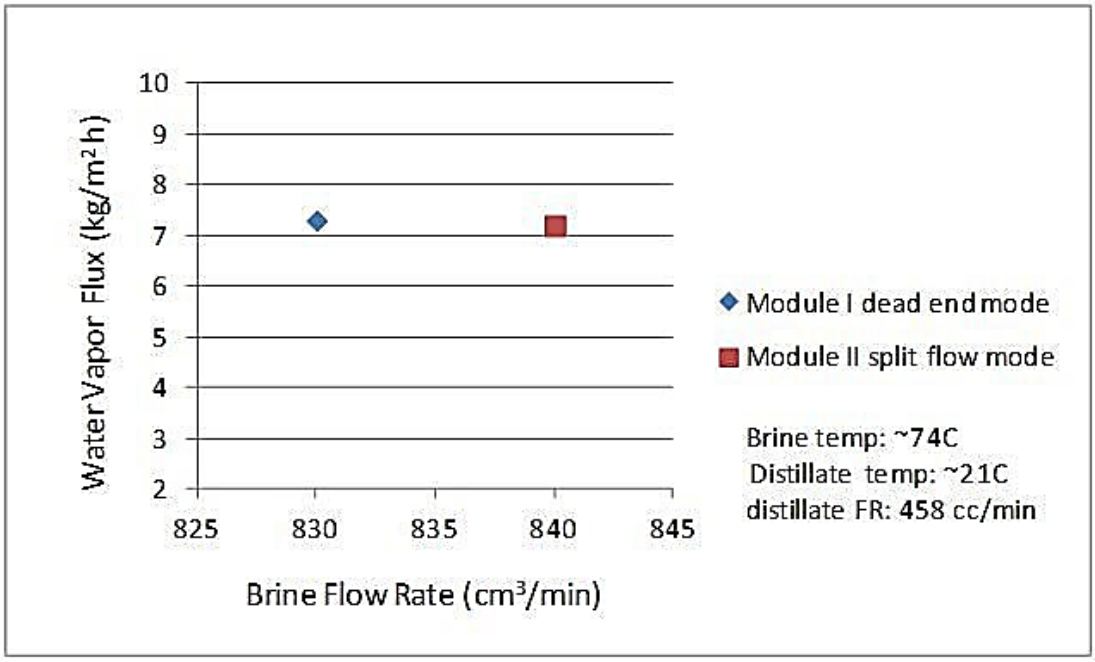

Figure 24.—Comparison of a water vapor flux with similar brine flow rate using large module I (Dead-End mode) and large module II (Split-Flow Mode); average distillate temperature ~21°C.

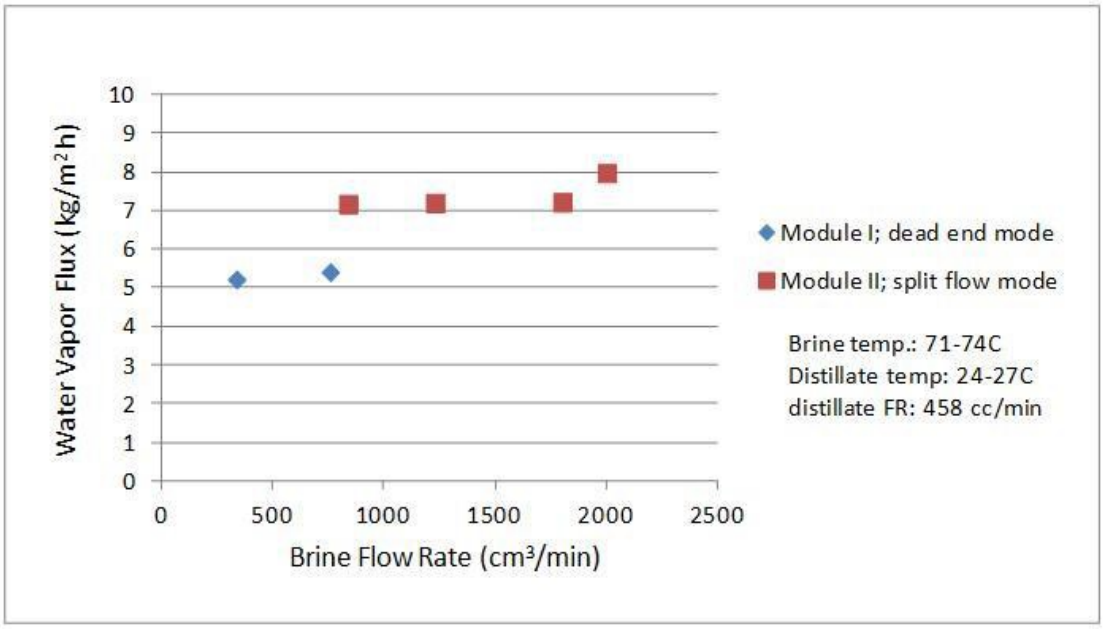

Figure 25.—Change in water vapor flux with different flow rates of 1% NaCl solution at 71-74°C in large module I (Dead-End Mode) and large module II (Split-Flow Mode); distillate in temperature at 24-27°C.

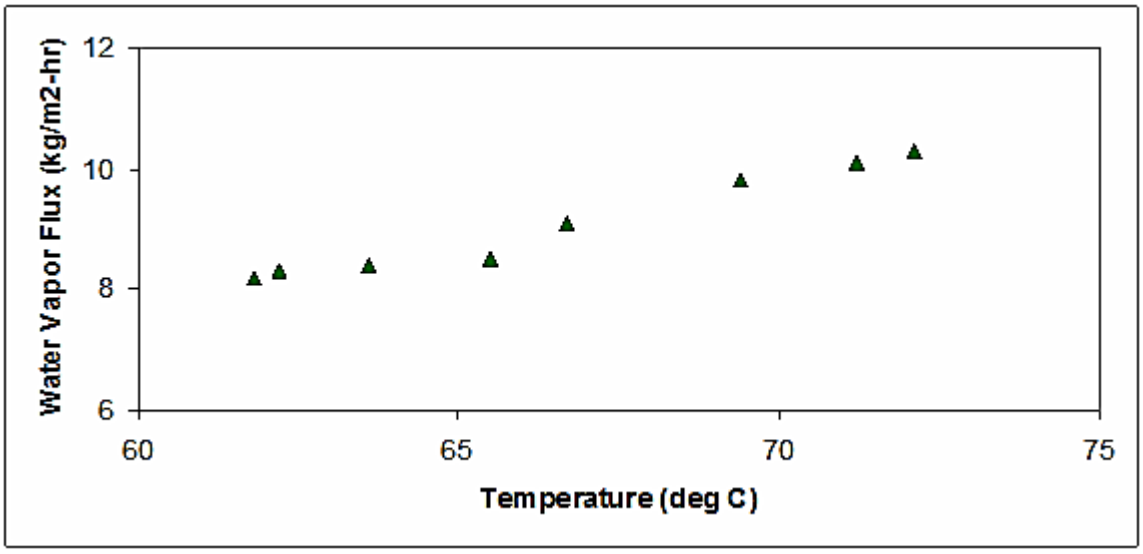

Figure 26.—Variation of water vapor flux in the large module I with change in brine temperature for a brine flow rate of 7.2 L/min (Split-Flow Mode) and a distillate flow rate of 0.5 L/min.

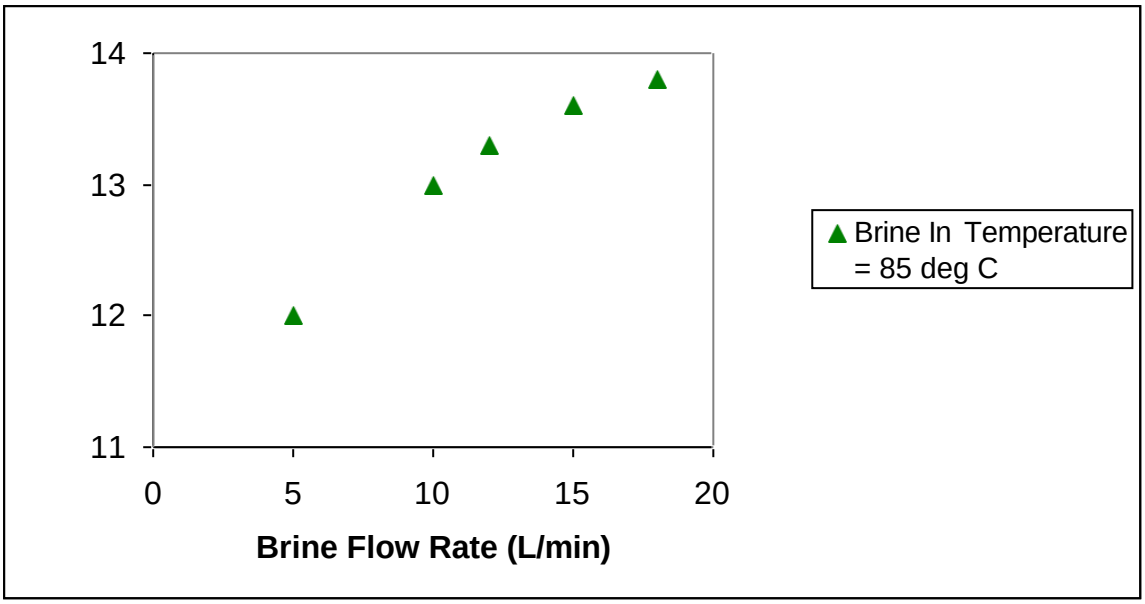

Figure 27.—Variation of water vapor flux with change in brine flow rate (Split-Flow Mode) for large module I for a brine-in temperature of 85°C.

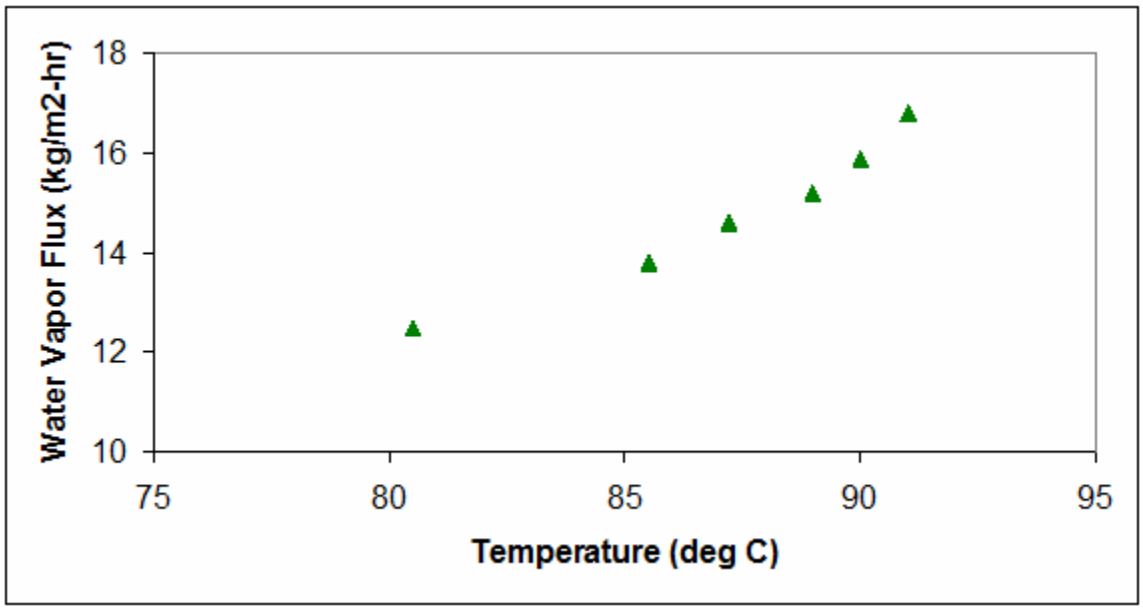

Figure 28.—Variation of water vapor flux with temperature for large module I having brine flow rate of 18 L/min (Split-Flow Mode) and distillate flow rate of 0.9 L/min.

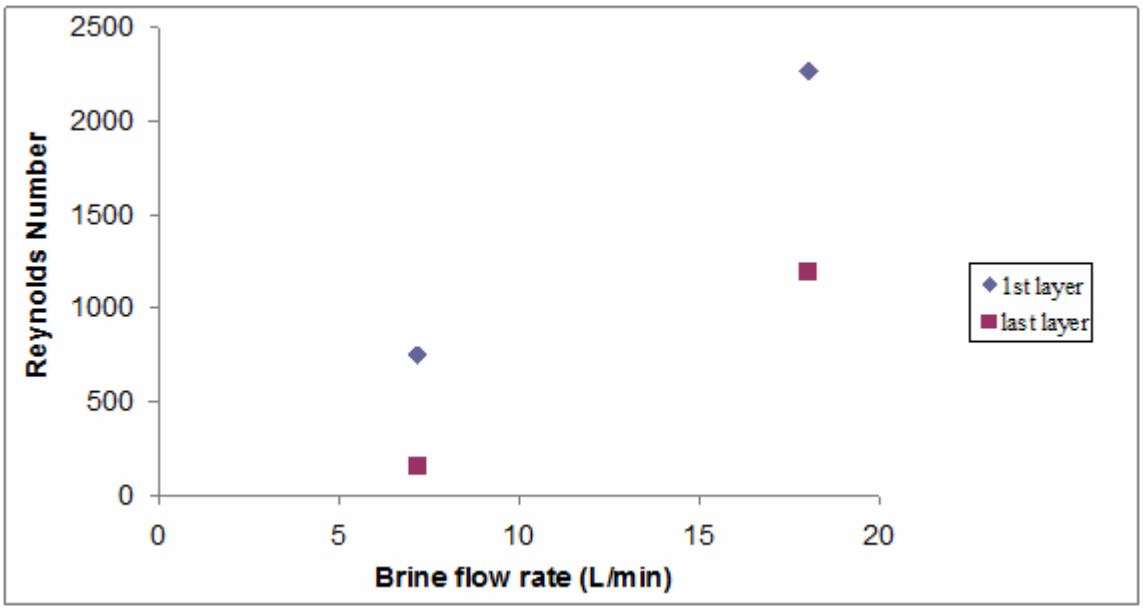

Figure 29.—Variation in Reynolds number with varying brine flow rate (Dead-End Mode) for different layers of large module I.

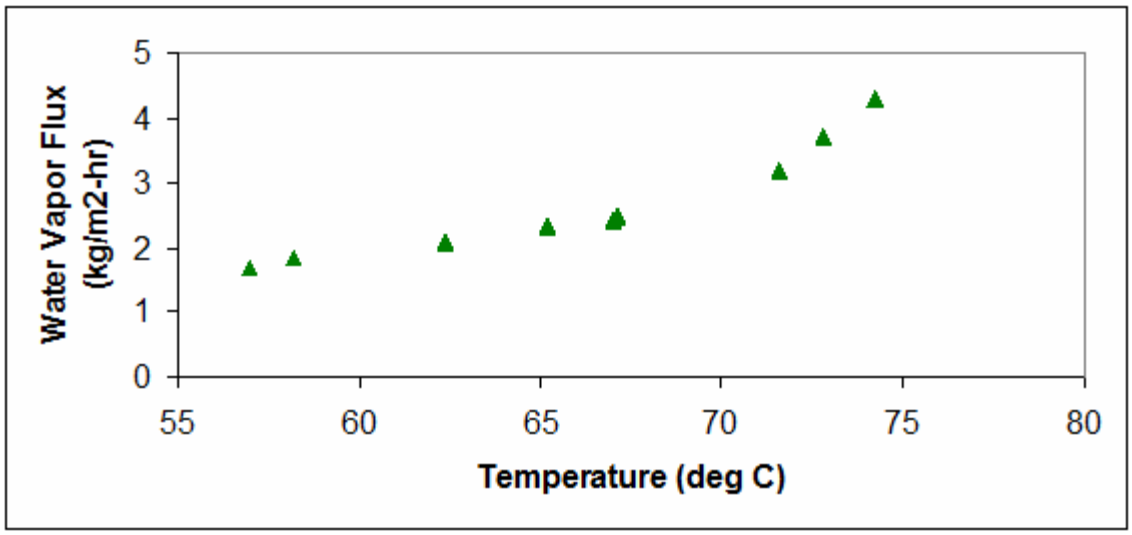

Figure 30.—Variation of flux with temperature for the large module III in the small DCMD experimental set up having a hot brine flow rate of 18 L/min (Split-Flow Mode) and a distillate flow rate 0.5 L/min.

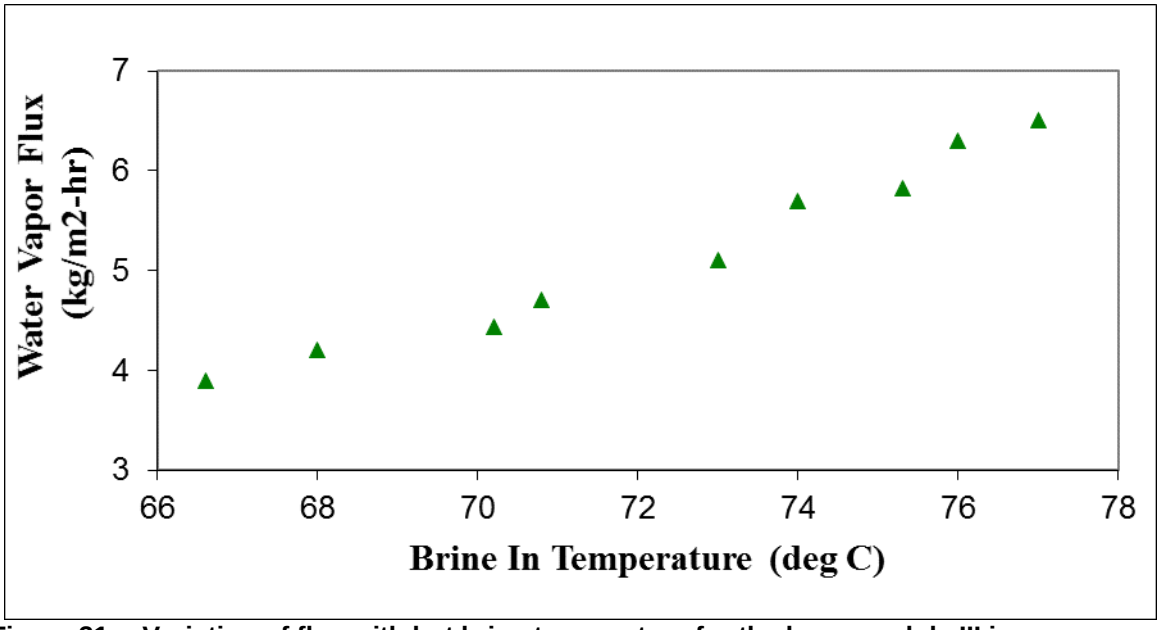

Figure 31.—Variation of flux with hot brine temperature for the large module III in the small DCMD experimental set up having a brine flow rate of 18 L/min (Split-Flow Mode) and a distillate flow rate of 0.9 L/min.

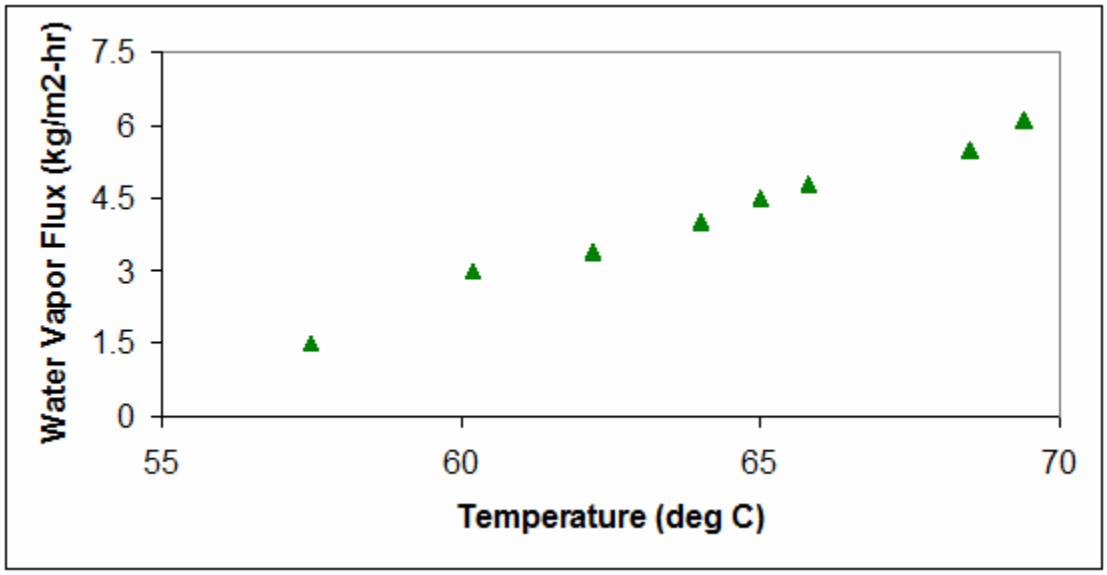

Figure 32.—Variation of water vapor flux with temperature for the large module III for a brine flow rate of 15 L/min (Split-Flow Mode) in the larger experimental setup.

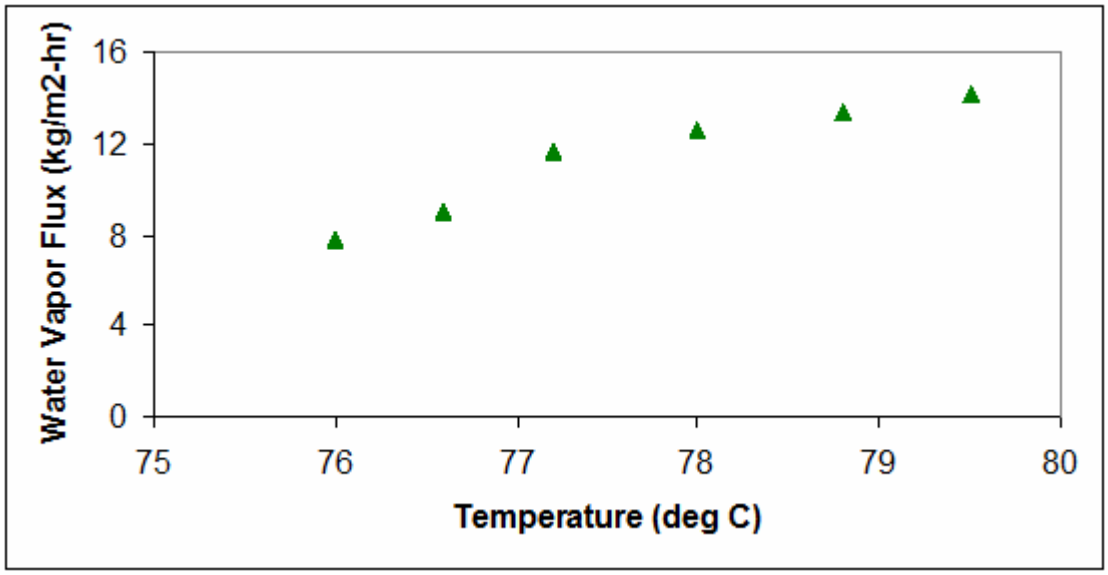

Figure 33.—Variation of water vapor flux with hot brine temperature for the large module III at a brine flow rate of 18 L/min (Split-Flow Mode) in the larger experimental setup.

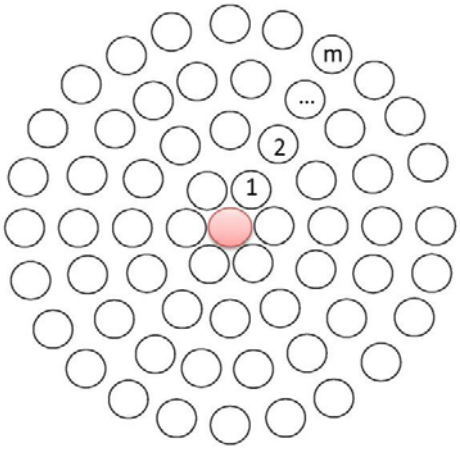

Figure 34.—Arrangement of fibers in the larger DCMD module.

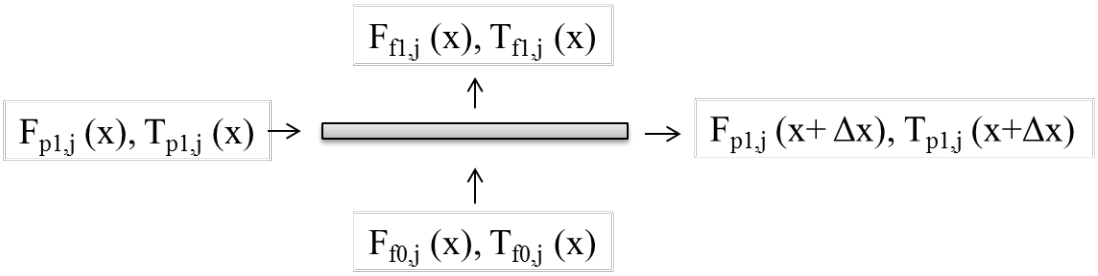

Figure 35.—Mass and energy balance for the length of Δx in the distillate flow direction.

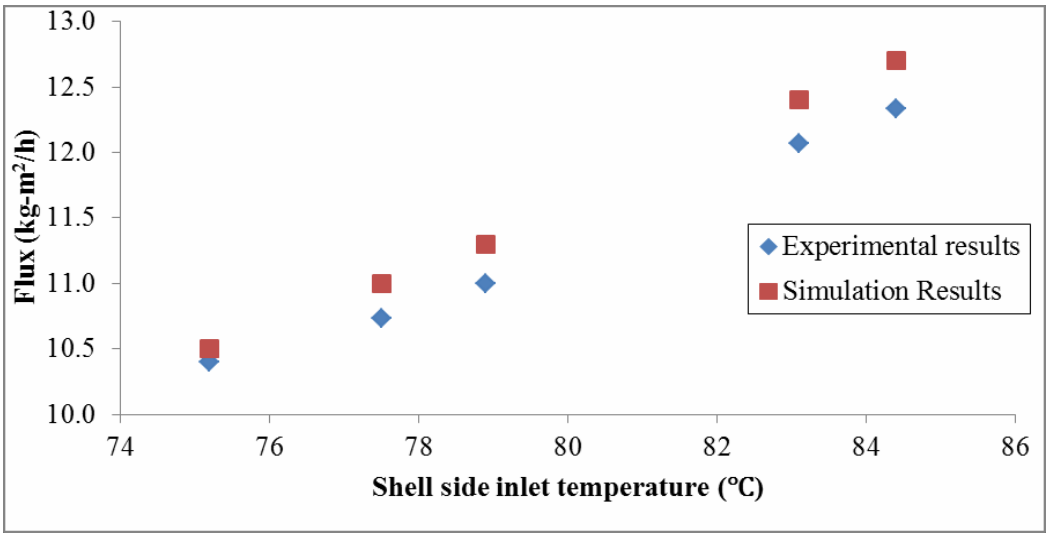

Figure 36.—Experimental and simulation results of the large module III. Hot feed brine is coming from one end of the central tube in the Dead-End Mode and the cooled brine is going out from both ends of the module. Cold distillate was in co-current flow with the hot feed brine. Shell side flow rate, 18 L/min; Tube side flow rate, 2.5 L/min; Shell side inlet temperature 75.2-84.4°C; Tube side inlet temperature 23.9-24.8°C; Brine inlet pressure 24.11-27.56 kPag (3.5-4 psig); Brine outlet pressure 0 kPag (0 psig); Distillate inlet pressure 99.90 kPag (14.5 psig); Distillate outlet pressure 0 kPag (0 psig).

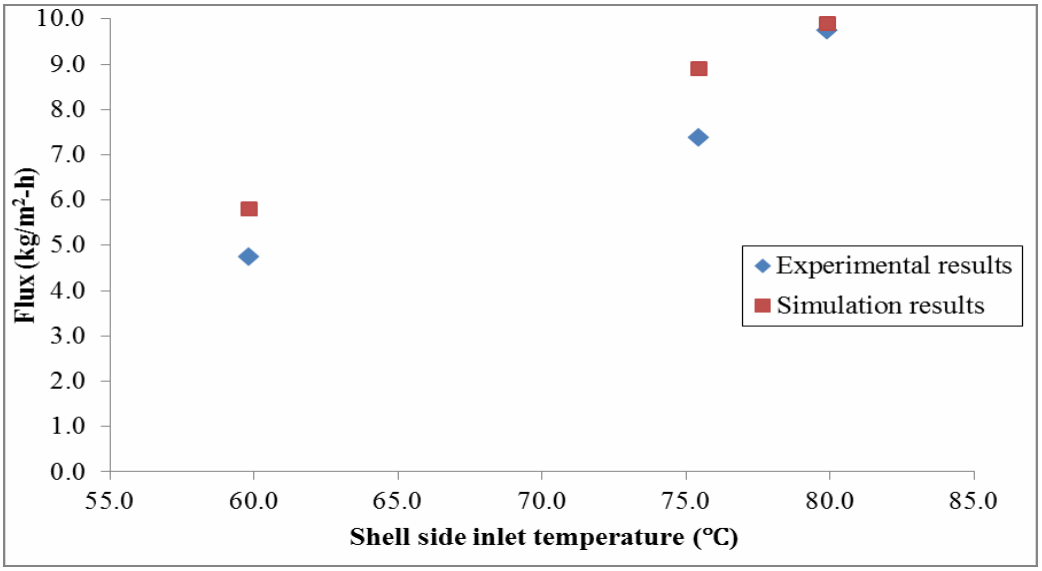

Figure 37.—Experimental and simulation results of the large module III for a lower brine flow rate. The hot feed brine feed is coming from one end of the central tube in Dead-End Mode and cooled brine is going out from both ends of the module. Cold distillate was co-current with the hot feed brine. Shell side flow rate, 15 L/min; Tube side flow rate, 2.5 L/min; Shell side inlet temperature 59.9-79.9℃; Tube side inlet temperature 24.1- 25.4℃; Brine inlet pressure 17.91-27.56 kPag (2.6-4 psig); Brine outlet pressure 0 kPag (0 psig); Distillate inlet pressure 65.45-99.90 kPag (9.5-14.5 psig); Distillate outlet pressure 0 kPag (0 psig).

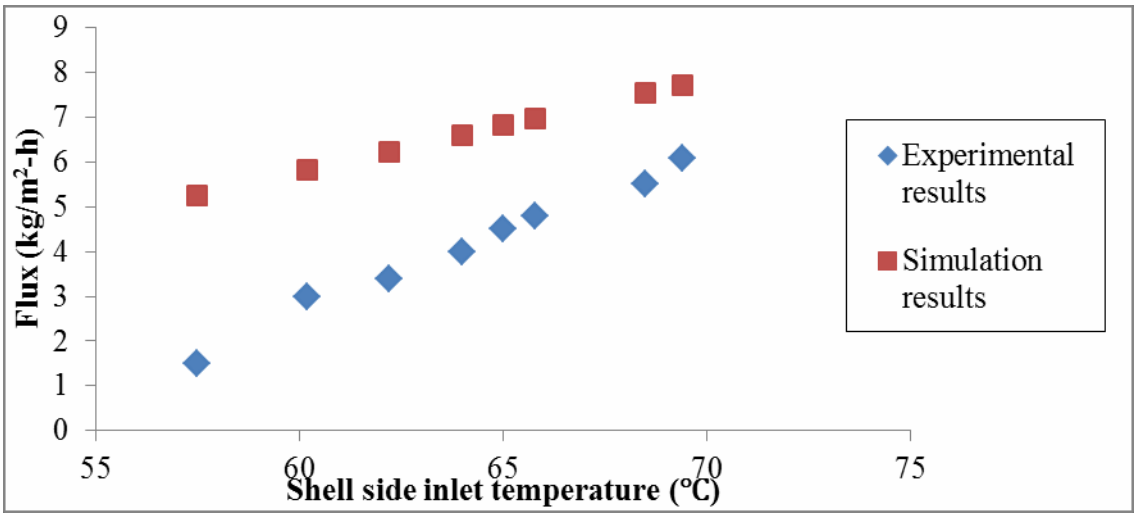

Figure 38.—Experimental and simulation results of large module III. Hot feed brine is coming from both ends of the central tube (Split-Flow Mode) and cooled brine going out from both ends of the module. Shell-side flow rate 15 L/min; Tube-side flow rate 2.5 L/min; Shell-side inlet temperature 58-70℃; Tube-side inlet temperature 23-25℃. Simulations are for Dead-End Mode.

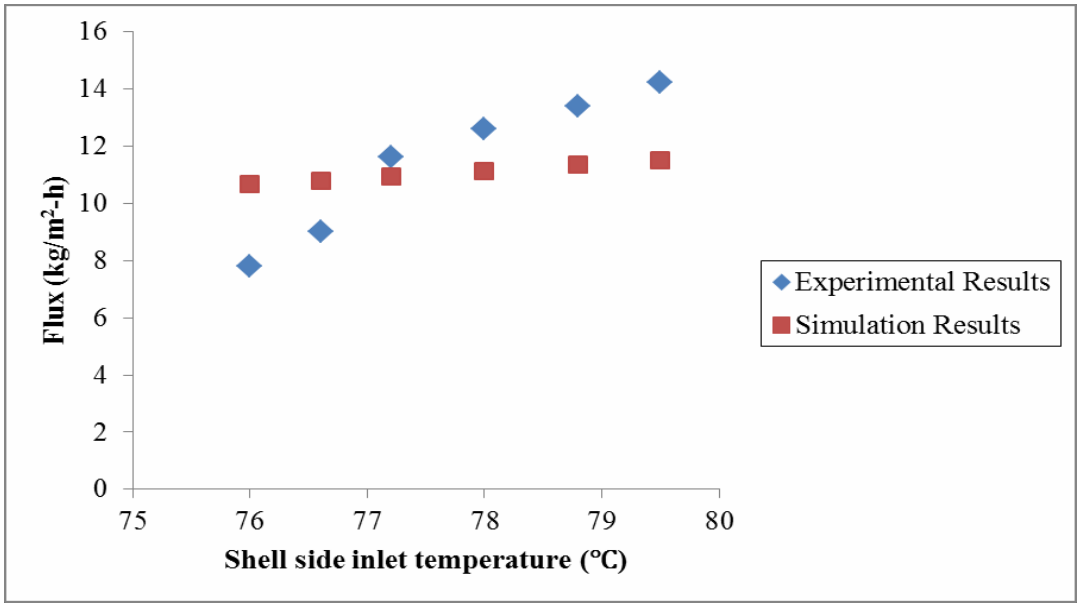

Figure 39.—Experimental and simulation results of large module III. Hot feed brine is coming from both ends of the central tube (Split-Flow Mode) and cooled brine going out from both ends of the module. Shell-side flow rate 18 L/min; Tube-side flow rate 2.5 L/min; Shell-side inlet temperature 76-80°C; Tube-side inlet temperature 23-25°C. Simulations are for Dead-End Mode.

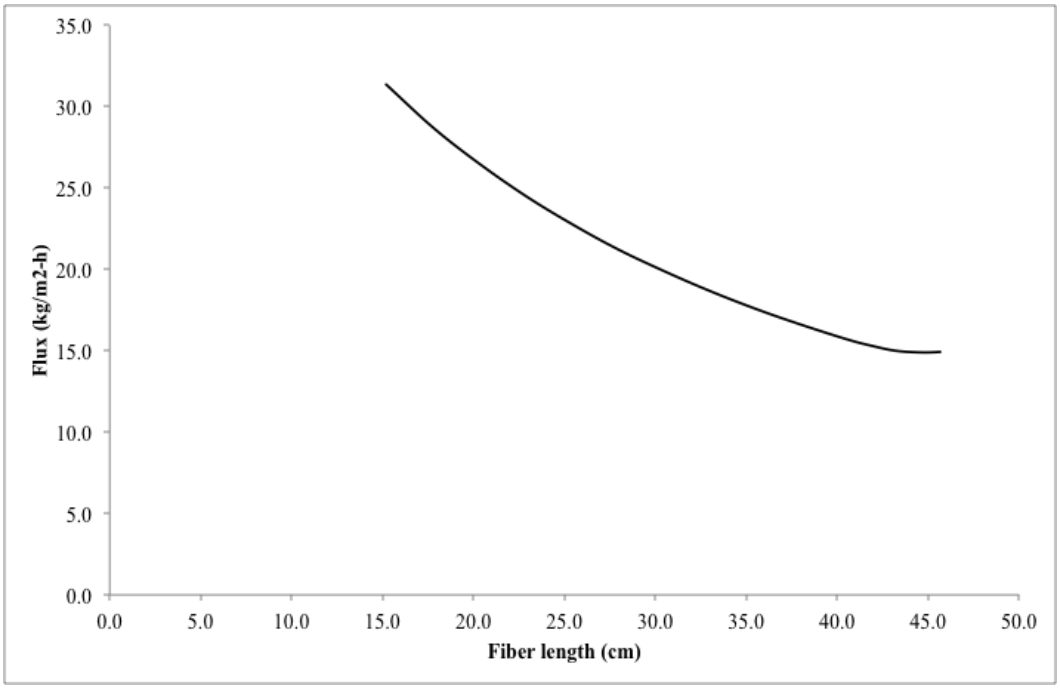

Figure 40.—Simulation results of Flux vs. fiber length for large module III, (Dead-End Mode). Shell side flow rate, 22.5 L/min. Tube side flow rate 2.5 L/min. Shell side inlet temperature 79.5 °C. Tube side inlet temperature 25.2 °C.

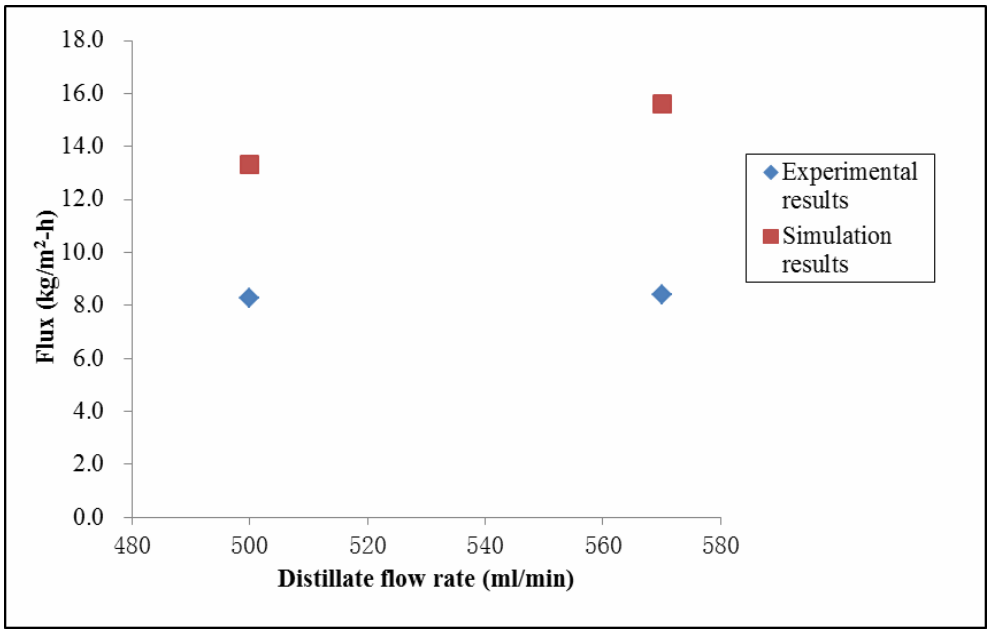

Figure 41.—Experimental and simulation results of the large module I. The hot feed brine is coming from both ends of the central tube (Split-Flow Mode) and cooled brine is going out from both ends of the module. Shell side flow rate, 5 L/min. Tube side flow rate varied. Shell side inlet temperature 62.2-63.6°C. Tube side inlet temperature 22.5-22.8°C. In the simulation, brine flow is in Dead-End Mode.

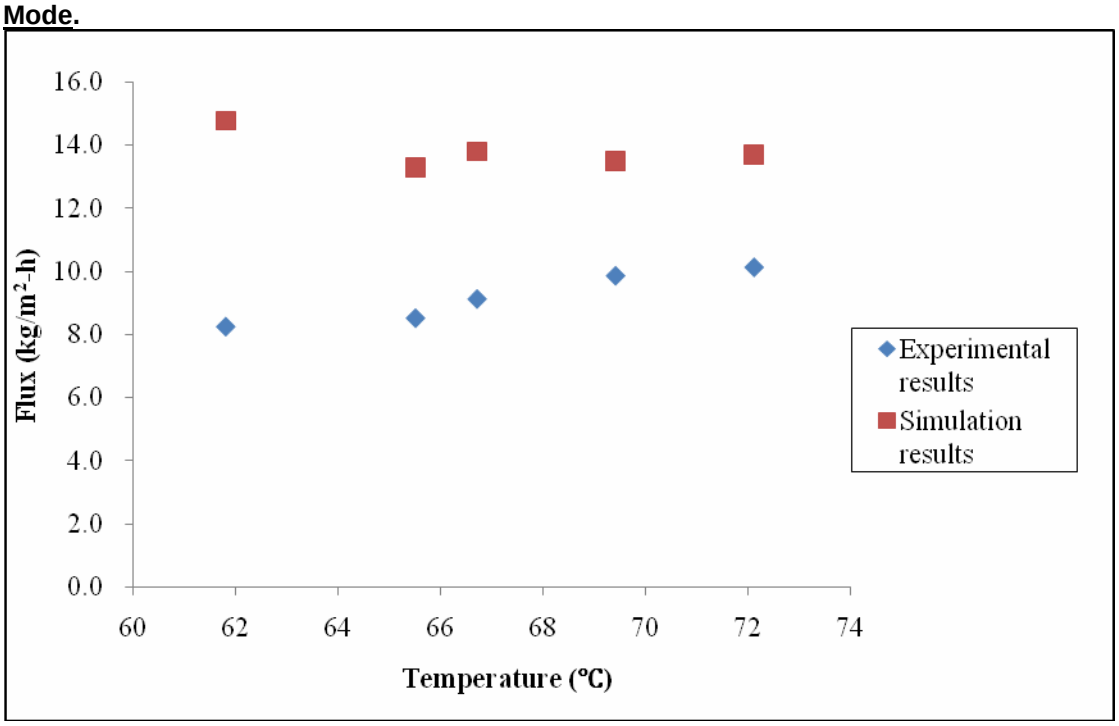

Figure 42.—Experimental and simulation results of large module I. Hot feed brine is coming from both ends of the central tube (Split-Flow Mode) and cooled brine going out from both ends of the module. Shell side flow rate 7.2 L/min. Tube side flow rate 0.57 L/min. Shell side temperature 61.8-72.1 °C. Tube side temperature 58.4-68.6 °C.

Appendix: Data tables

Table A.1.—Detailed experimental results for large module III in dead-end mode shown in Figure 36

Tbi	Tbo	Tdi	Tdo	Fbi	Fdi	Overflow mass flow rate	Average overflow mass flow rate	Flux
℃	℃	℃	℃	L/min	L/min	mL/h	mL/h	kg/m2-h
75.2	68	24.2	30.8	18	2.5	6220	6233.3	10.4
						6240		
						6240		
77.5	70.4	24.2	31.4	18	2.5	6440	6440.0	10.7
						6440		
						6440		
78.9	71.6	23.9	31.4	18	2.5	6600	6606.7	11.0
						6620		
						6600		
83.1	75.5	24.8	31.9	18	2.5	7220	7233.3	12.1
						7240		
						7240		
84.4	76.1	24.8	32.4	18	2.5	7400	7406.7	12.3
						7420		
						7400		

Table A.2.—Detailed experimental results for large module III in dead-end mode shown in Figure 37

Tbi	Tbo	Tdi	Tdo	Fbi	Fdi	Overflow mass flow rate	Averag e overflo w mass flow rate	Flux
℃	℃	℃	℃	L/min	L/min	mL/h	mL/h	kg/m2-h
59.9	55.1	24.1	27.1	15	2.5	2880	2866.7	4.8
						2860		
						2860		
75.5	70.2	25.4	31.3	15	2.5	4450	4433.3	7.4
						4450		
						4400		
79.9	72.0	25.4	31.3	15	2.5	5860	5866.7	9.8
						5860		
						5880		

Table A.3.—Experimental data for Figure 17

Brine In Temperature (deg C)	Water Vapor Flux (kg/m^2-hr)
84.5	2.5
85.7	4.0
86.0	4.2

Table A.4.—Experimental data for Figure 18

Brine Flow Rate (ml/min)	Water Vapor Flux (kg/m2-hr)
800	2.3
1000	2.6
1500	3.0
1800	4.2

Table A.5.—Experimental data for Figure 19

Brine In Temperature (deg C)	Water Vapor Flux (kg/m2-hr)
85	4.2
90	6.0
91	6.6

Table A.6.—Experimental data for Figure 20

Brine In Temperature (deg C)	Brine Flow Rate (ml/min)	Water Vapor Flux (kg/m^2-hr)
85	800	3.1
	1500	4.5
	1800	5.9
90	800	5.3
	1500	9.0
	1800	9.9

Table A.7.—Detailed experimental results for Figure 22 for points for large module II in dead-end mode

Tbi/Tbo (°C)	Tdi/Tdo (°C)	Fbi (cc/min)	Fdi (cc/min)	Overflow Mass Flow Rate (cm3/min)	Total time (min)	Flux* (cm3/cm2min)	Flux (kg/m2h)
64.8/57.9	22.0/31.2	7000.00	458.00	600	294	1.52E-02	9.12
64.8/57.3	22.6/32.1	"	"	782			
58.6/53.0	22.7/31.9	"	"	744			
61.4/57.1	22.2/31.4	"	"	626			
61.8/57.7	22.3/31.7	"	"	762			
61.7/57.8	22.6/31.6	"	"	670			
63.6/59.6	22.7/32.1	"	"	876			
62.7/58.7	22.8/32.1	"	"	770			
63.6/59.0	22.7/32.0	"	"	874			

* Flux calculated as total volume collected over total time and membrane area based on membrane ID

Table A.8.—Detailed experimental results for Figure 22 for data points for large module II in split-flow mode

Tbi/Tbo (°C)	Tdi/Tdo (°C)	Fbi (cc/min)	Fdi (cc/min)	Overflow Mass Flow Rate (cm3/min)	Total time (min)	Flux* (cm3/cm2min)	Flux (kg/m2h)
71.1/56.0	21.1/28.3	1220.0	458.00	600	98	1.28E-02	7.68
72.7/57/1	21.5/29.5	"	"	668			
69.9/55.1	21.4/29.4	"	"	614			
69.1/50.2	24.0/28.0	840.0	458.00	970	168	1.09E-02	6.55
71.8/52.4	22.6/28.9	"	"	1004			
74/53.9	22.3/28.9	"	"	779			

* Flux calculated as total volume collected over total time

Table A.9.—Detailed experimental data for Figure 22 for data points for large module I in dead-end mode

Tbi/Tbo (°C)	Tdi/Tdo (°C)	Fbi (cc/min)	Fdi (cc/min)	Overflow Mass Flow Rate (cm3/min)	Total time (min)	Flux* (cm3/cm2min)	Flux (kg/m2h)
67.4/22.7	22.8/24.	114.27	458.00	168	210	1.76E-03	1.06
64.6/23.0	21.7/24.	"	"	178			
63.6/23	20.3/24.	"	"	208			
67.6/22.7	22.7/24.	256.65	458.00	184	286	2.68E-03	1.61
66.1/41.3	23.0/24.	"	"	183			
67.6/40/6	24.2/25.	"	"	210			
66.1/39.8	23.5/25.	"	"	206			
66.3/40.7	23.5/25.	"	"	186			
66.7/22.8	24.2/25.	"	"	182			
62.0/32/0	26.0/28.	395.3	458.00	214	253	3.38E-03	2.03
69.5/32.1	25.0/28.	"	"	486			
61.5/31.9	25.2/28.	"	"	260			
61.8/31.9	25.4/28.	"	"	324			

* Flux calculated as total volume collected over total time and membrane area

Table A.10.—Detailed experimental results for Figure 23 for data points on large module I in dead-end mode at 57 °C

Tbi/Tbo (°C)	Tdi/Tdo (°C)	Fbi (cc/min)	Fdi (cc/min)	Overflow Mass Flow Rate (cm3/min)	Total time (min)	Flux* (cm3/cm2min)	Flux (kg/m2h)
59.1/31.7	24.7/26.7	330.0	458.00	220	246	3.68E-03	2.21
63.4/34.8	27.9/29.1	"	"	436			
54.4/32.8	25.6/29.1	"	"	246			
56.7/32.9	25.6/29.1	"	"	200			
56.0/33.4	25.7/29.3			257			

Table A.11.—Detailed experimental results for Figure 23 for data points on large module I in dead-end mode at 74 °C

Tbi/Tbo (°C)	Tdi/Tdo (°C)	Fbi (cc/min)	Fdi (cc/min)	Overflow Mass Flow Rate (cm3/min)	Total time (min)	Flux* (cm3/cm2min)	Flux (kg/m2h)
76.5/36.9	33.4/31.4	340.0	458.00	564	252	6.50E-03	3.90
74.4/35.7	33.0/30.4	"	"	630			
-	-	"	"	594			
75.0/35.9	32.9/30.8	"	"	669			

Table A.12.—Detailed experimental data for Figure 24 for data points on large module I in dead-end mode at 74 °C for a higher brine flow rate

Tbi/Tbo (°C)	Tdi/Tdo (°C)	Fbi (cc/min)	Fdi (cc/min)	Overflow Mass Flow Rate (cm3/min)	Total time (min)	Flux* (cm3/cm2min)	Flux (kg/m2h)
74.5/54.4	23.8/28.1	830	458.00	1030	120	1.22E-02	7.30
72.7/53.6	22.8/28.8	"	"	1160			

Table A.13.—Detailed experimental data for Figure 24 for data points for large module II in split-flow mode at 74 °C

Tbi/Tbo (°C)	Tdi/Tdo (°C)	Fbi (cc/min)	Fdi (cc/min)	Overflow Mass Flow Rate (cm3/min)	Total time (min)	Flux* (cm3/cm2min)	Flux (kg/m2h)
69.2/50.5	20.8/27.1	840	458.00	600	210	1.20E-02	7.2
72.0/52.3	21.4/28.0	"	"	750			
73.4/53.0	21.4/27.8	"	"	692			
73.5/53.0	21.6/28.1	"	"	576			
73.6/53.0	21.6/28.5	"	"	544			
69.2/50.5	20.8/27.1	"	"	604			

Table A.14.—Detailed experimental data for Figure 25 for data points for large module I in dead-end mode at 71-74 °C

Tbi/Tbo (°C)	Tdi/Tdo (°C)	Fbi (cc/min)	Fdi (cc/min)	Overflow Mass Flow Rate (cm3/min)	Total time (min)	Flux* (cm3/cm2min)	Flux (kg/m2h)
76.9/34.3	30.9/29.6	340	458.00	466	120	8.71E-03	5.23
77.2/35.4	31.9/30.4	"	"	507			
-	-	"	"	606			
76.5/36.9	33.4/31.4	760	458.00	788	121	9.01E-03	5.41
72.4/52.9	17.9/30.3	"	"	848			

Table A.15.—Detailed experimental data for Figure 25 for data points for large module II in split-flow mode at 71-74 °C

Tbi/Tbo (°C)	Tdi/Tdo (°C)	Fbi (cc/min)	Fdi (cc/min)	Overflow Mass Flow Rate (cm3/min)	Total time (min)	Flux* (cm3/cm2min)	Flux (kg/m2h)
69.2/50.5	20.8/27.1	840	458.0	600	210	1.20E-02	7.17
72.0/52.3	21.4/28.0	"	"	750			
73.4/53.0	21.4/27.8	"	"	692			
73.5/53.0	21.6/28.1	"	"	576			
73.6/53.0	21.6/28.5	"	"	544			
-	-	"	"	604			
71.3/56.5	21.9/28.8	1230.0	458.0	650	254	1.20E-02	7.22
72.8/57.3	22.3/29.3	"	"	736			
63.0/51	20.7/29.0	"	"	563			
65.4/52.4	20.1/28/4	"	"	422			
68.2/54.2	20.9/29.1	"	"	526			
70.3/55.8	21.7/29.7	"	"	500			
71.7/56.7	22.2/30.4	"	"	606			
72.6/57.3	22.1/30.4	"	"	582			
73.6/50.7	23.5/31.5	1800.0	458.0	656	271	1.41E-02	8.44
73.4/50.7	23.4/32.1	"	"	648			
72.6/50.9	23.1/32.2	"	"	634			
72.0/51.3	22.6/31.8	"	"	612			
71.6/51.3	22.5/31.8	"	"	646			
72.6/52.2	23.0/32.2	"	"	580			
72.5/53.5	22.8/32.3			656			
71.8/59/2	22.7/31.7	2000.0	458.0	650	277	1.33E-02	7.97
73.3/59.8	22.8/32.0	"	"	678			
74.0/60.7	24.2/33.7	"	"	660			
74.6/61.0	24.1/33.7	"	"	762			
65.5/54.8	22.5/32.7	"	"	606			
66.7/55.4	21.4/31.5	"	"	494			
69.6/57.4	22.1/31.4	"	"	516			
71.5/58.9	22.7/31.3	"	"	540			
72.6/58.9	23.0/32.0	"	"	610			

Table A.16.—Experimental data for Figure 26

Brine In Temp (deg C)	Water Vapor Flux (kg/m2-hr)
61.8	8.2
62.2	8.3
63.6	8.4
65.5	8.5
66.7	9.1
69.4	9.8
71.2	10.1
72.1	10.3

Table A.17.—Experimental data for Figure 27

Brine In Flow Rate (Lt/min)	Water Vapor Flux (kg/m2-hr)
5	12.0
10	13.0
12	13.3
15	13.6
18	13.8

Table A.18.—Experimental data for Figure 28

Brine In Temp (deg C)	Water Vapor Flux (kg/m2-hr)
80.5	12.5
85.5	13.8
87.2	14.6
89.0	15.2
90.0	15.9
91.0	16.8

Table A.19.—Experimental data for Figure 30

Brine In Temp (deg C)	Water Vapor Flux (kg/m2-hr)
57.0	1.7
58.2	1.8
62.4	2.1
65.2	2.3
67.0	2.4
67.1	2.5
71.6	3.2
72.8	3.7
74.2	4.3

Table A.20.—Experimental data for Figure 31

Brine In Temp (deg C)	Water Vapor Flux (kg/m2-hr)
66.6	3.9
68.0	4.2
70.2	4.4
70.8	4.7
73.0	5.1
74.0	5.7
75.3	5.8

Table A.21.—Experimental data for Figure 32

Brine In Temp (deg C)	Water Vapor Flux (kg/m2-hr)
57.5	1.5
60.2	3.0
62.2	3.4
64.0	4.0
65.0	4.5
65.8	4.8
68.5	5.5
69.4	6.1

Table A.22.—Experimental data for Figure 33

Brine In Temp (deg C)	Water Vapor Flux (kg/m2-hr)
76.0	7.8
76.6	9.0
77.2	11.6
78.0	12.6
78.8	13.4
79.5	14.2